Fermilab

TM-826
2750.000

CONCEPTUAL DESIGN OF A LARGE, THIN COIL SUPERCONDUCTING SOLENOID MAGNET FOR COLLIDING BEAM EXPERIMENTS AT FERMILAB

D. Cline*, W. Craddock, R. Fast (editor), D. Gross, H. Kautzky, E. Leung, B. Strauss

Fermi National Accelerator Laboratory
Batavia, Illinois 60510

R. Niemann, R. Smith, L. Turner

Argonne National Laboratory
Argonne, Illinois

J. Rhoades, W. Young

University of Wisconsin
Madison, Wisconsin

Preliminary: September 5, 1978
Final: October 25, 1978

ABSTRACT

A large (3m ϕ x 5m x 1.5T) superconducting solenoid has been conceptually designed. The magnet uses a calorimeterized pole and yoke and discrete flux return legs to provide a uniform magnetic field inside the solenoid and low field outside. The coil and cryostat have a thickness of $\sim$ 0.6 radiation lengths. High purity aluminum is soldered to the conductor for stability and quench protection. The magnet and refrigerator are designed for a five minute charge time. Details of the quench study, structure analysis, and cooldown calculations are given. The report of an independent design review committee is included.

TABLE OF CONTENTS

I. INTRODUCTION

A. General Physics Goals of the Solenoid Detector

In the near future, colliding beam experiments will become possible at Fermilab. There are two distinct types of interaction that can be studied: (a) $\bar{p}p$ collisions at a center of mass energy of 400 or 2,000 GeV;[1] (b) pp collisions at a center of mass energy up to 1,200 GeV.[2] In light of these possibilities, a group of physicists have considered various magnetic detector configurations for use as a Colliding Detector Facility.[3] A solenoid magnet and detector with very thin coil was recommended by this group. In this report, we have undertaken a conceptual design of this magnet.

There are several reasons for choosing a solenoid magnet, one of which is the inherent simplicity of the magnetic field because of the cylindrical symmetry of the coil. The parameters of the magnet are set by the desired charged particle momentum resolution and the required angular coverage for a special class of high energy induced events that are produced with an intermediate vector boson. It is expected that the detector will be rather versatile and provide information about a broad class of "central" collisions between very high energy particles.

Another physical requirement was that the coil be extremely thin so that electrons and photons have a high probability of passing through without radiating. This allows the placement of large shower counters outside the coil. Furthermore, we required that the

magnetic field just outside the coil be kept very low (< 100 gauss) so that ordinary photomultipliers can be operated there. The large field free region is expected to be useful for other types of particle detectors as well. Finally, it must be possible to charge the magnet in five minutes or less.

In order to meet these requirements, two important conditions arise:

1. The magnet coil must be superconducting since no other material has such a large current to thickness ratio.
2. The magnetic flux return must be far (2m) from the coil on the sides.

The most serious question raised by these requirements was the feasibility and cost of such a magnet. A second question of importance was the ability to service particle detectors internal to the magnet. Figure I-1 shows a schematic drawing of the coil and flux return configuration.

B. General Features of the Magnet

The following conceptual design report describes a magnet with the following characteristics:

diameter = 3m

length = 5m

$|\vec{B}|$ = 1.5T

thickness $\leq$ 0.6 radiation lengths

Special laminated iron end caps and four discrete iron flux-return legs provide an extremely uniform field within the solenoid for simplified determination of particle momenta, to enable hadron calorimetry within the end cap regions, and to provide low field regions just

SOLENOID MAGNET DETECTOR (Fermilab)

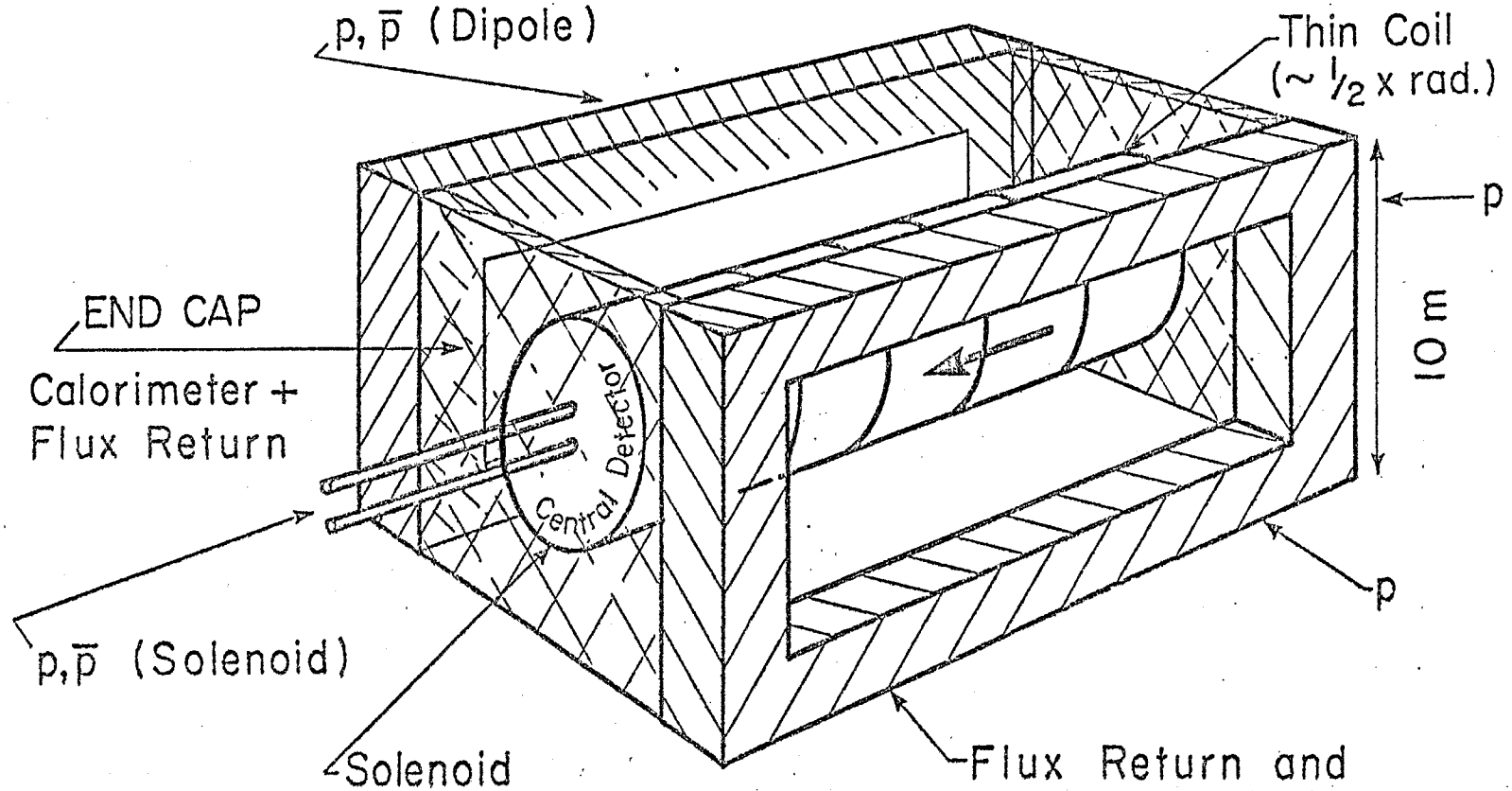

B = 1.5T
d = 3.0m
ℓ = 5m

Energy stored = 25 MJ

Solenoid Dipole Magnet Configuration

Figure I-1

outside the coil for photomultipliers. A forced-flow closed-tube cooling system coupled with careful cryostat design based on established cryogenic engineering techniques will assure ease of operation of the system while physics research is underway.

The report contains sections on each of the magnet components. A summary of the system parameters may be found in Section VI. An Appendix, Section X, contains the detailed calculations. Section XI is the report of an independent Review Committee which studied this design. The recommendations of the Review Committee are not implemented here.

In the report the internal and external particle detectors for the facility will not be discussed. Nevertheless, the access to the internal detectors, especially in a limited space provided by a colliding beam interaction area, is of crucial importance. The access will be made through the removal of an end cap cone. An exploded view of the detector assembly is shown in Figures I-2a through 2d. We have not considered any support structure for the internal detector or the external detector. Furthermore, the detailed design of the end cap Fe calorimeter configuration is left to another group.

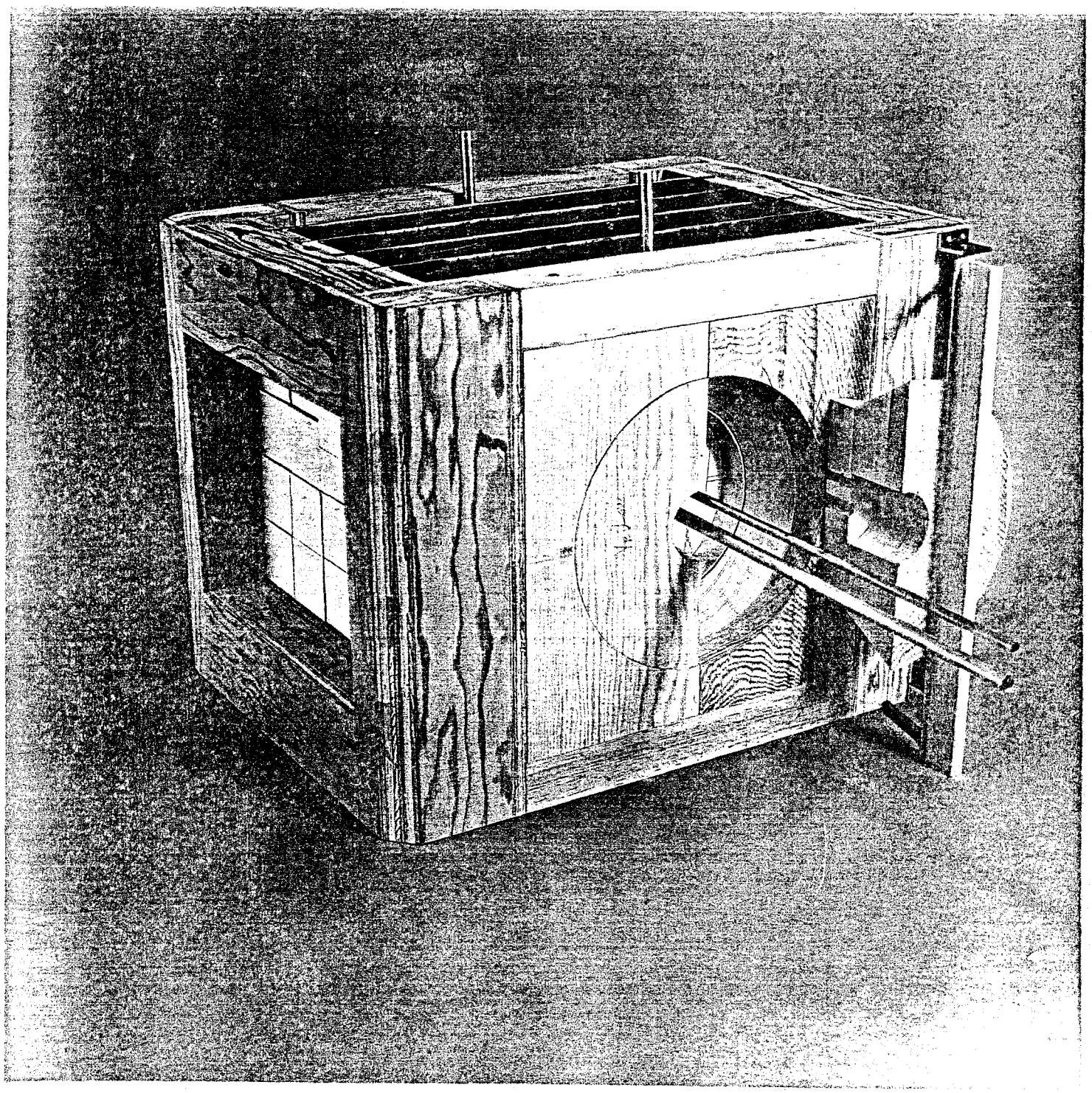

Figure I-2a

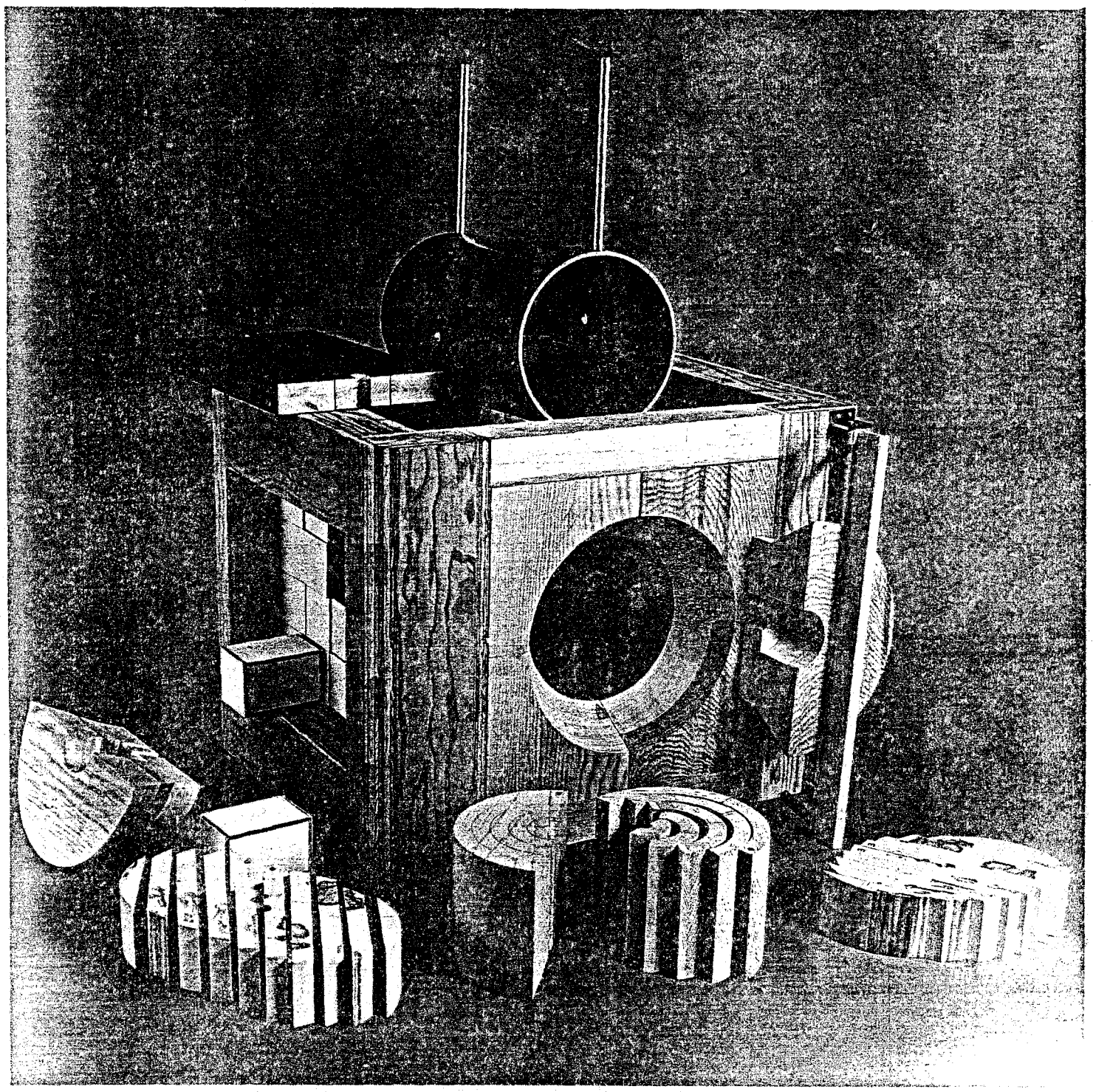

Figure I-2b

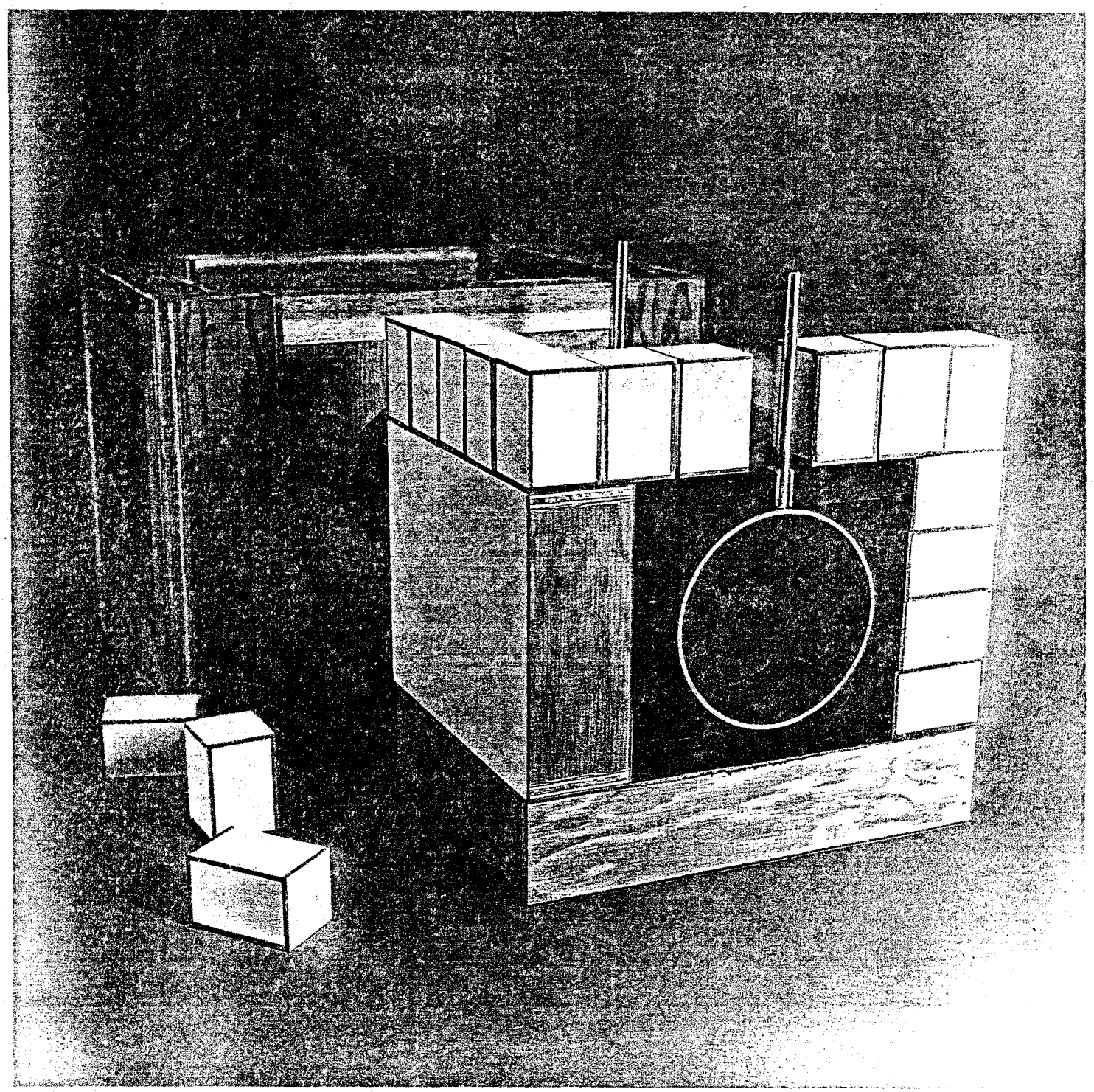

Figure I-2c

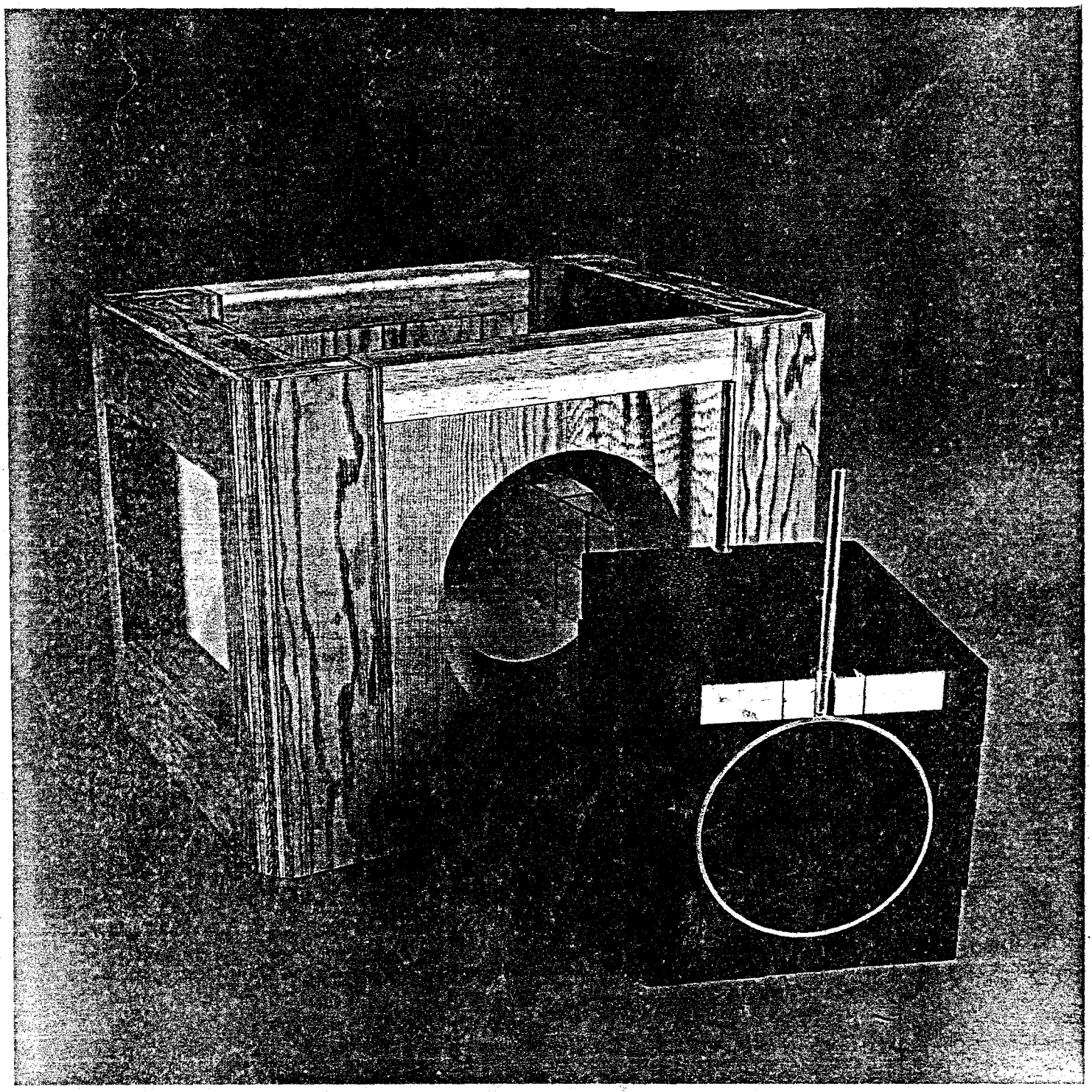

Figure I-2d

REFERENCES

1. D. Cline, P. McIntyre, F. Mills, and C. Rubbia, "Collecting Antiprotons in the Fermilab Booster and Very High Energy $\bar{p}p$ Collisions", Fermilab TM 689 (1976); D. Cline, "Possibility for Antiproton-Proton Colliding Beams at Fermilab", CERN $\bar{p}p$ Note 08, May, 1977. E. Gray et al., Proceedings of the 1977 Accelerator Conference, IEEE Transaction Vol. NS 24, 3 1954 (1977).

2. Private communication from D. Cline, B. Richter, and C. Rubbia to R.R. Wilson, 1975. Fermilab Proposals P-492 and P-493.

3. C. Ankenbrandt, M. Atac, G. Chadwick, W. Chen, D. Cline, R. Diebold, R. Fast, I. Gaines, H. Kautzky, B. Kells, P. McIntyre, F. Mills, B. Musgrave, T. Rhoades, R. Singer, B. Strauss, F. Turkot, J. Walker, R. Yamada, "Preliminary Design of a Magnetic Detector Facility for Colliding Beams at Fermilab", CDF-11, May, 1978.

II. COIL DESIGN

A. General Features

To insure that the magnet will reach the design field of 1.5T and operate reliably at that level, a conductor directly stabilized with low resistivity aluminum has been chosen. Such a conductor shows excellent self-protection in the event of a quench, and recent experience at CEN-Saclay[1] shows that a solenoid of this size constructed of such a conductor could probably reach the short-sample limit without training or other degrading effects. The rapid charge rate (300 sec) required for the magnet precludes the use of a highly conductive bobbin for quench protection.

The expense of fabricating a built-up conductor made from a conventional Cu/NbTi superconducting wire continuously soldered to a shunt of high purity aluminum provides important benefits of safety and reliability for the magnet. With the low resistivity metal electrically and thermally intimate with the superconductor, no inductive or other "active" quench protection circuits are required. The axial and circumferential quench velocities[2,3] of such a conductor are sufficiently high that the use of a parallel dump resistor is adequate to prevent the development of destructive temperatures on quench. The value of the dump resistor can be chosen so that both the hot spot temperature and internal and terminal voltages are comfortably low.

The copper and aluminum matrix material, in intimate thermal contact with the superconductor, should provide

sufficient stability for a tube-cooled coil to reach an operating point 75 - 80% along the load line without quenching.

An overall linear current density (current per unit axial length of coil) of 1200 A/mm (12kA/cm) is required to generate a central field of 1.5T.

B. Conductor Design

The operating current of the magnet is chosen to be 5,000 Amperes. Calculations made with the program QUENCH[4] show this current to give small internal voltages and low temperatures during a magnet quench. Other advantages to this current include a modest (40V) charging voltage, reduced coil winding labor cost, and decreased probability of shorts. Furthermore, the steady-state conduction and radiation heat load of approximately 10 watts will vaporize sufficient liquid helium to provide adequate cold gas for two 5,000A vapor-cooled leads. Thus, no operating penalties are incurred by this choice of current.

The Cu/NbTi composite will be fabricated with a Cu:NbTi ratio of 1.8:1. The size of the composite (with 10% extra linear current density and 0.2mm turn-to-turn insulation) is 2.0 mm x 3.59 mm; other parameters are given in Section VI. The magnet load line and composite short sample curves are shown in Figure II-1.

In order to size the pure aluminum strip to which the Cu/NbTi composite is soldered, it was decided to choose the same ratio of operating current to aluminum area as used in the Saclay-CELLO conductor, i.e., 16.7 kA/cm^2. For a 5,000A conductor, this amounts to

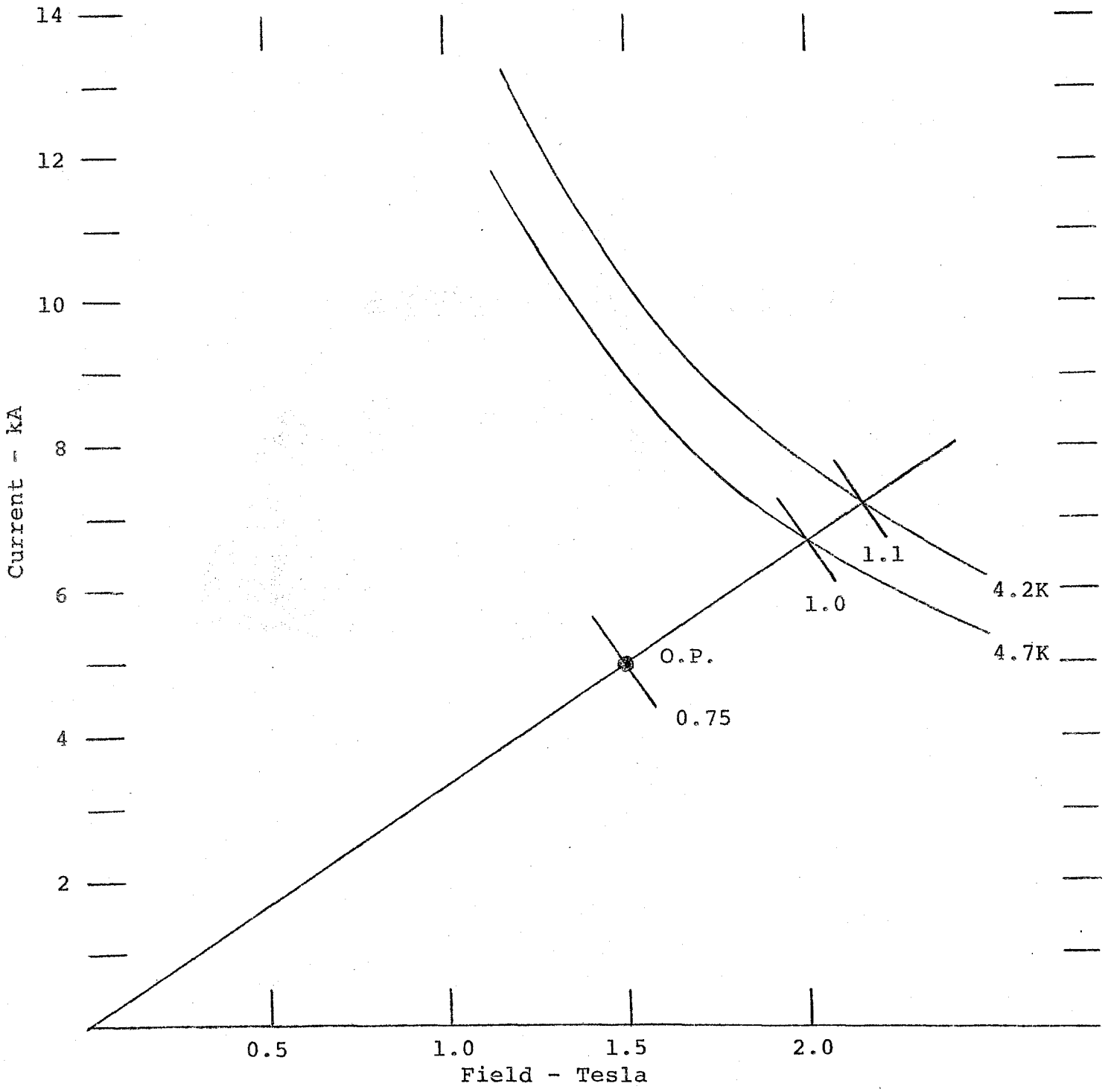

FIG. II-1

MAGNET LOAD LINE & SHORT SAMPLE LINES

$30mm^2$ of pure aluminum area, with dimensions of 3.59mm x 8.36mm.

The overall Al/Cu/NbTi conductor is 3.59mm x 10.36mm, and has an area ratio of 11.7:1.8:1. The conductor could be insulated with Kapton, Mylar, or B-stage epoxy glass tape. Film insulations, such as Formvar, can not be used due to their high curing temperature.

Raw material for the Cu/NbTi composite would be purchased from the Fermilab stockpile and fabricated to the required final size. The heat treatment to optimize the short sample performance will be performed at an earlier stage (larger diameter) in the fabrication process than for Tevatron conductor. The solder bonding process will use the method developed at Saclay for the CELLO conductor. The aluminum is copper, electroplated, then electrotinned and bonded to the tinned composite by a continuous induction heating assembly line. An ultrasonic technique continuously monitors the quality of the joint. Several American manufacturers have indicated a willingness to perform the soldering. CEN-Saclay has also offered to fabricate the conductor, using the equipment and techniques used for the CELLO conductor.

C. Stability Considerations

The stability of the conductor-coil system, i.e., its ability to withstand heat pulses without quenching, has been considered. Potential sources of heat include inelastic mechanical processes, especially during charging, and charging eddy current heating. Since the coil is

tube-cooled rather than bath-cooled a large, quickly responsive liquid helium heat sink is unavailable. Stability must, therefore, come from minimizing the heat sources and using the high purity aluminum as an enthalpy sink.

The time constant for the current to move from the superconducting composite into the high purity aluminum is about one second. The time constant for a heat pulse to move into the aluminum is several orders of magnitude less. It is the large thermal diffusivity that provides stability for sufficiently small heat pulses. The thermal and electrical properties of the aluminum must be controlled during the lifetime of the magnet in order to maintain a large thermal diffusivity. Specifically, the magneto-resistivity and cyclic-strain resistivity of the aluminum must be carefully considered in the design of the coil.

Recent data[5] (Figure II-2) on the cyclic-strain resistivity of high purity aluminum, for example, shows that the resistivity rises dramatically when the cyclic strain exceeds 0.2 - 0.3%. The magneto-resistance (Figure II-3) of high purity aluminum[6] suggests that the aluminum be located in a field-free region if possible i.e., outside the Cu/NbTi composite. For high purity aluminum at low strain, with B = 0.0T, for example, about one microsecond is required to dissipate a heat pulse. If B = 2.0T, this time nearly triples. For a choice of aluminum of "commercial high purity" (e.g., 1100 alloy with RRR $\sim$ 100) or even high

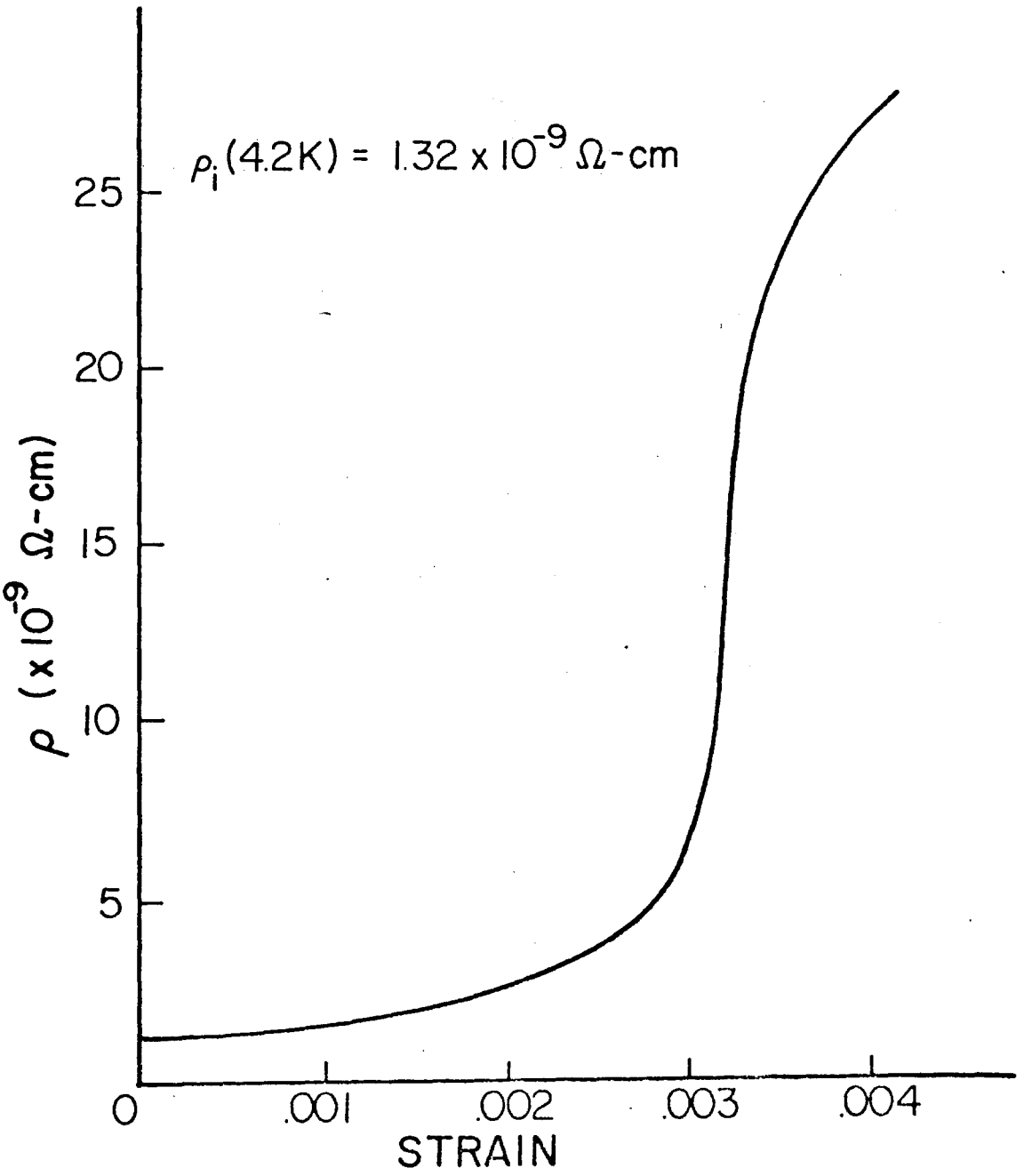

FIG. II-2

Resistivity after 1,000 cycles vs. strain for reinforced, high purity aluminum. Initial RRR of the high purity aluminum was 2,000.

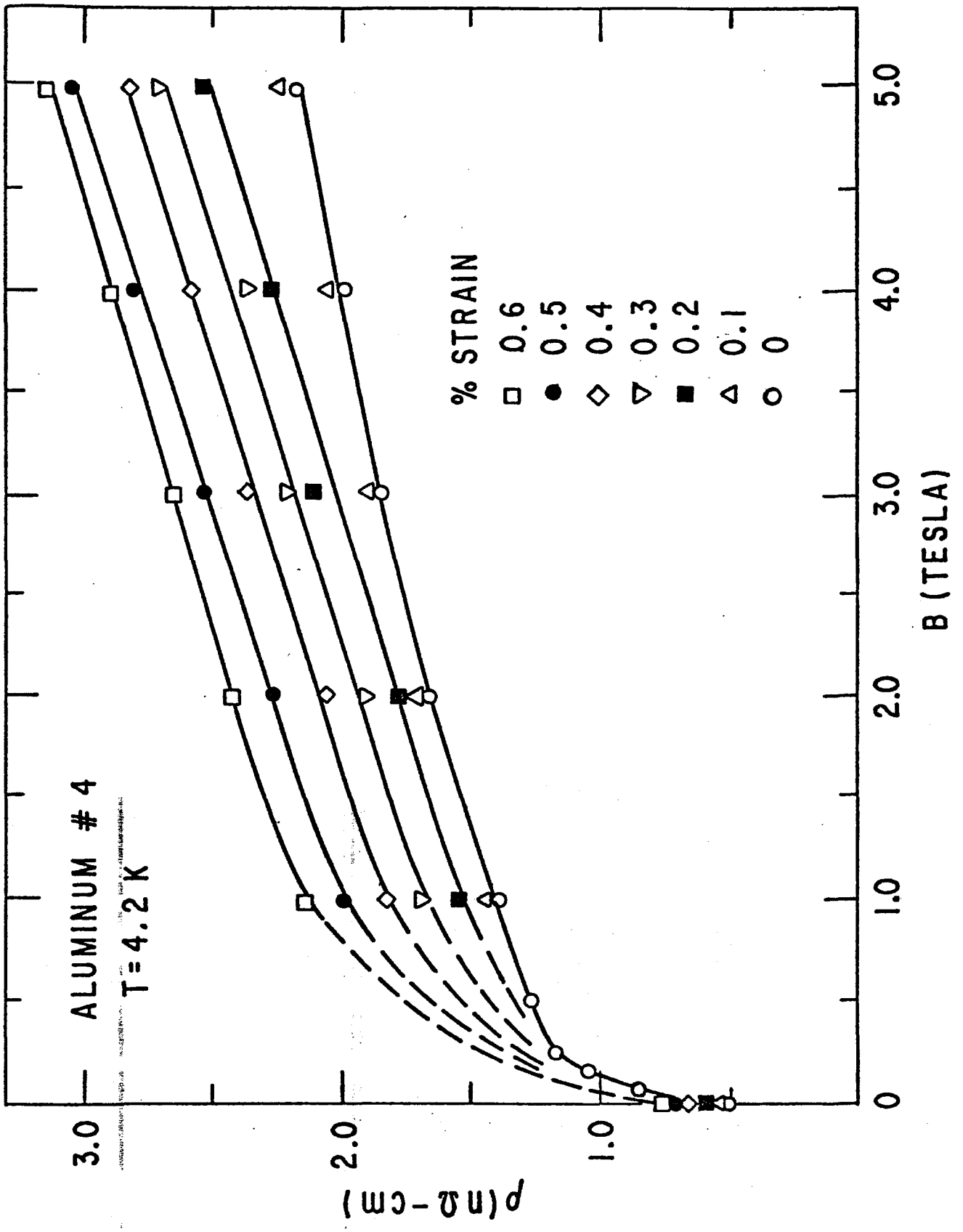

FIG. II-3

MAGNETO-RESISTIVITY OF HIGH-PURITY ALUMINUM

purity aluminum at large cyclic strain, this time increases by an order of magnitude. The relative significance of these times is as follows. For a given heat pulse (from e.g., a mechanical perturbation) the safety margin is reduced by an order of magnitude in the last instance, and even by a factor of about three if high purity aluminum is in the magnetic field instead of outside it.

In summary, stability considerations resulted in a stabilizer of high purity aluminum (99.99+%, RRR > 1,000), located in a field free region with a maximum strain of 0.2%. The coil design must be as free of latent sources of mechanical heat pulses as possible.

D. Quench Considerations

Quench considerations result in several general coil design objectives. The axial quench propagation velocity, turn-to-turn across a dielectric layer, is very important for quench safety. The internal and terminal voltages are also important. It is desirable, therefore, to have minimum turn-to-turn insulation and coil-to-ground insulation adequate for several kilovolts.

E. Coil Winding Design

The coil is a single layer, with the conductor spiral wound with the narrow edge against the bobbin. Support structure for the electromagnetic forces is provided by aluminum alloy outside the coil, to which the cooling tubes are attached. Three coil design alternatives are discussed and the quench characteristics of each

given in paragraph III-F.

CELLO - Style Coil Design - Prestressed Coil and Banding (Figure II-4a)

The conductor is wound on an aluminum alloy bobbin over a layer of epoxy-wetted fiberglass cloth with the Cu/NbTi composite against the bobbin. Since there is little flux outside the current sheet, there is negligible eddy current heating in the high purity aluminum during charging. Furthermore, since there is essentially no field in the aluminum, magneto-resistance effects are negligible. Prestressed banding insures contact between the bobbin and the conductor at all times.

The bobbin of high strength aluminum alloy must be slit axially with a fiberglass strip (loaded always in compression) to eliminate eddy current heating when charging the coil. Without this slit the heating is 300 Watts.

The outward radial magnetic pressure at 1.5T of 0.9MPa(130 psi) is supported by the outer aluminum banding the conductor and the bobbin such that the strain in the high purity aluminum does not exceed 0.2% when the magnet is energized. Details of the stress analysis of bobbin, coil, and banding are given in Appendix X-A. The bobbin is 1.1 cm (0.433") thick and the banding is 1.03cm (0.406") thick. The coil is loaded axially during winding and clamped on completion to maintain tightness within the coil. This precompression exceeds the outward axial load on the windings due to magnetic forces during quench. The strain introduced

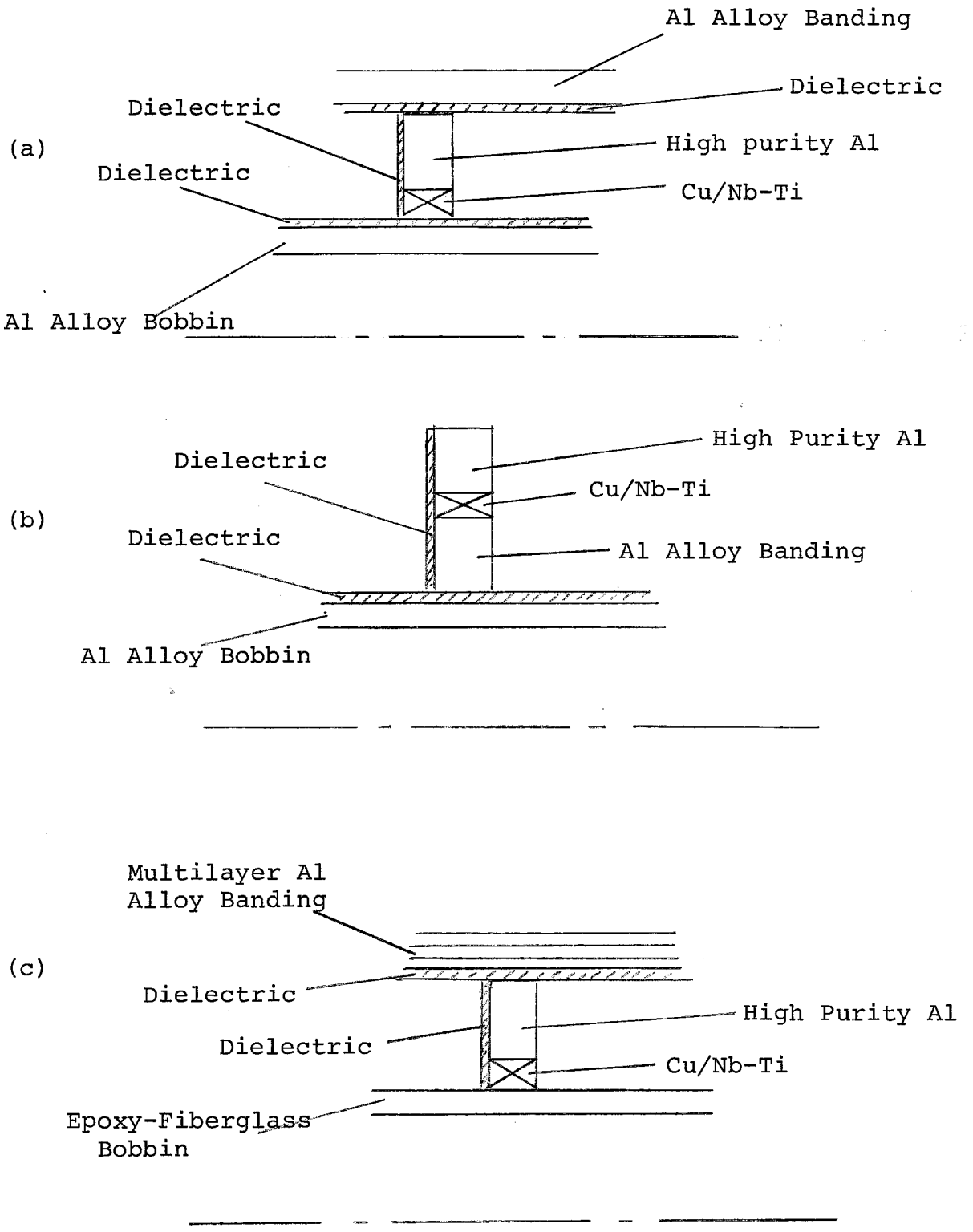

FIG. II-4

ALTERNATE COIL DESIGNS

into the high purity aluminum from coil winding and banding will be annealed out after the winding is completed, as the layup epoxy is cured at about 100°C.

A few joints (on the order of 10) are anticipated in the coil, the number depending on fabricational details of the conductor. A soldered lap joint of 30cm will have a resistance of 1×10^{-9} ohms giving a power dissipation of 25mW, at least one order of magnitude below the heating tests carried out on the Saclay test coil.[7]

It is proposed to return the conductor from the far end of the coil alongside and thermally intimate with the cooling tube so that both ends of the conductor, as well as both ends of the cooling tube, can exit the cryostat in a single penetration.

No Prestress Design -

Integral Conductor and Banding (Figure II-4b)

The hoop stress on the conductor can be restrained with a support structure having no prestress. To limit the strain in the coil to 0.2%, a stress of:

$$\sigma = \varepsilon E = 0.002 \times (11 \times 10^6) = 22 \text{ Ksi} = 152\text{MPa}$$

must exist in the support structure. If the design pressure is 10% greater than the magnetic load, and the contribution of the conductor ignored, the banding thickness is:

$$t = pr/\sigma = 143\text{psi} \times 56"/22\text{ksi} = 0.364\text{in}$$

$$= 0.923\text{cm}$$

The support must be mechanically intimate with the

conductor before the coil is energized so that the strain is controlled and conductor motion precluded. The structure consists of a high strength aluminum strip co-soldered to the conductor and wound against the bobbin. This conductor/structure composite would be wound on the bobbin with no winding tension. Since no radial preload would exist in the winding, there would be no radial buckling stresses on the bobbin. An aluminum alloy bobbin thickness of 3mm (0.118") is thick enough to support the axial preload required for winding and stiff enough to react the axial decentering force to the vacuum vessel. Since eddy current heating during charge is 90 watts, it may be possible to eliminate the slit in the bobbin. The conductor neutral axis is near the Cu/NbTi component, so that the winding prestrain in the high purity aluminum does not greatly exceed that of the prestressed design. There is no magnetic flux in the high purity aluminum so the thermal diffusivity is identical to that of the prestressed design. Eddy current heating in the high-strength alloy during charge is negligible. The magnetic hoop stress is easily sustained by the solder bonds in the conductor.

No Prestress Design -

Large Sheet Banding (Figure II-4c)

This design uses an epoxy/fiberglass bobbin, on which the basic conductor is wound without tension. The support structure is provided by aluminum sheets wrapped without prestress around the outside of the coil and epoxied together. The stress analysis is given in Appendix X-B. Approximately 5mm of banding is required.

The layered banding gives excellent axial integrity to the coil and provides the needed axial precompression and stiffness.

A comparison of the three coil designs is given in Table II-1. It is obvious that it is possible to combine some of the features into a composite design, e.g., the use of an epoxy/fiberglass bobbin with prestressed banding.

F. Quench Behavior

Our design philosophy is that the probability of coil damage following a full field quench initiated by any mechanism (e.g., loss of vacuum or refrigeration) be essentially zero. H. DesPortes has calculated[8] CELLO to have a very safe quench behavior. All three of our coil designs use a CELLO-style conductor. Considering the electrical circuit shown in Figure II-5, the program QUENCH[9] has been used to study the quench process for each of the coil designs. It was recognized very early in the study that due to the 10 meter circumference, the turn-to-turn axial growth of a normal zone was at least as important and perhaps more important than axial growth along the conductor. The study thus far has used quench velocities in these two directions comparable to those measured for the CELLO conductor[10] and on the Saclay model[11], i.e., $\sim$ 12m/sec along the conductor and $\sim$ 30 cm/sec transverse.

The program was used to assist with the choice of current. As the results of Table II-2 show, a 5,000A design has lower hot spot temperatures and smaller

TABLE II-1

MAGNET STRUCTURE - A COMPARISON OF THREE DESIGNS

	1	2	3
Construction	Slit aluminum bobbin	Epoxy fiberglass bobbin	Epoxy fiberglass bobbin
Description	Prestressed spiral band structure	Structure soldered to conductor, no winding stress	Bonded sheet structure, no prestress
Principal Advantages	Both radial & axial clamping Minimal tension in conductor Little concern for differential contraction	Excellent thermal properties Aluminum stabilizer is stressed very little	Ease of manufacturing attachments to bobbin Minimal eddy current problems
Possible Problems	Loss of prestress Difficult to attach spiral banding to end flanges Insulated break in bobbin	Winding radius of conductor must be formed <u>before</u> soldering of structure	Difficult to assure axial clamping Match of contraction coefficients

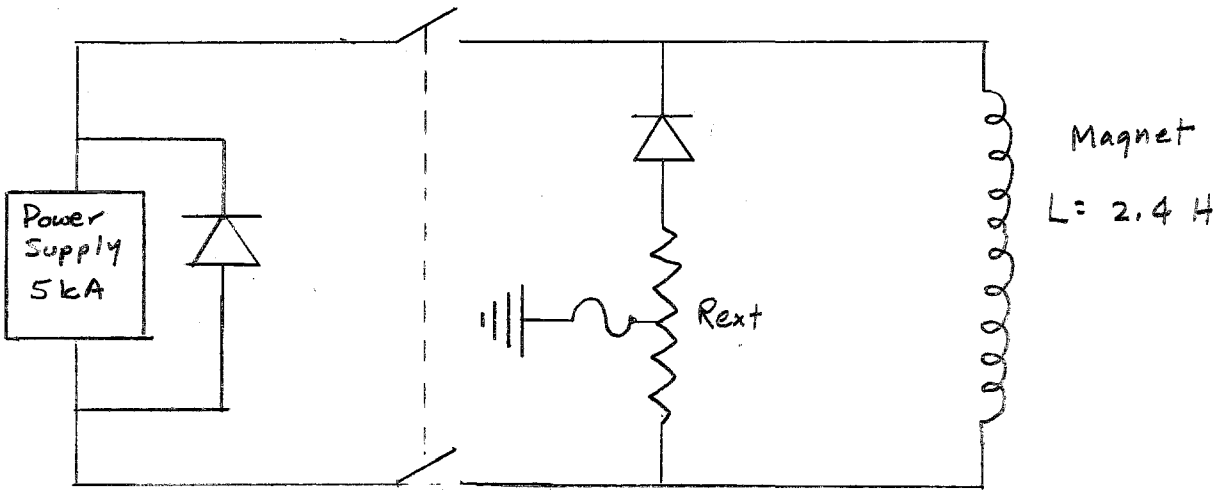

FIG. II-5

POWER SUPPLY - MAGNET CIRCUIT

TABLE II-2

QUENCH CHARACTERISTICS vs. MAGNET CURRENT

No Banding

Operating Current	3400 A	5100 A
Discharge time constant τ	7.3 sec	7.2 sec
Fractional energy removed	50.0%	69.8%
Maximum hot spot temperature	388 K	308 K
Maximum resistive internal voltage	2160 V	889 V

internal voltages than a 3400A design. In order to get a feel for the dependence of hot spot temperature and internal voltage on the values of the external resistor and quench velocities, a series of QUENCH runs was made ignoring the banding and assuming that the current transfers instantaneously into the high purity aluminum. The results are shown in Figure II-6,7, and 8.

The actual current sharing behavior of the copper and high purity aluminum has been modeled. The thermal properties of the conductor included the aluminum at all times, but the current was not allowed to spread into the aluminum instantaneously once the normal front passed, but rather it was allowed to diffuse into the full metal cross section with the magnetic diffusivity $\tau_{mag} = \frac{4\mu_0}{\pi^2} \frac{w^2}{\rho}$, which has a value with $\rho = 1.2 \times 10^{-9}$ Ω-cm of 1.1 sec for B = OT and 0.35 sec for B = 2T. Table II-3 shows the effect of current sharing between the copper and aluminum, still ignoring the banding.

The coil designs which use aluminum banding separated electrically and thermally from the conductor can be worst case modeled by ignoring the banding. The data of Table II-3 is, therefore, representative of these coil designs. In the coil design in which the banding was soldered to the conductor the banding provides both a well coupled thermal mass and a shunt current path. Table II-4 shows that in general the hot spot temperature is somewhat less and the voltage significantly less if this technique is used.

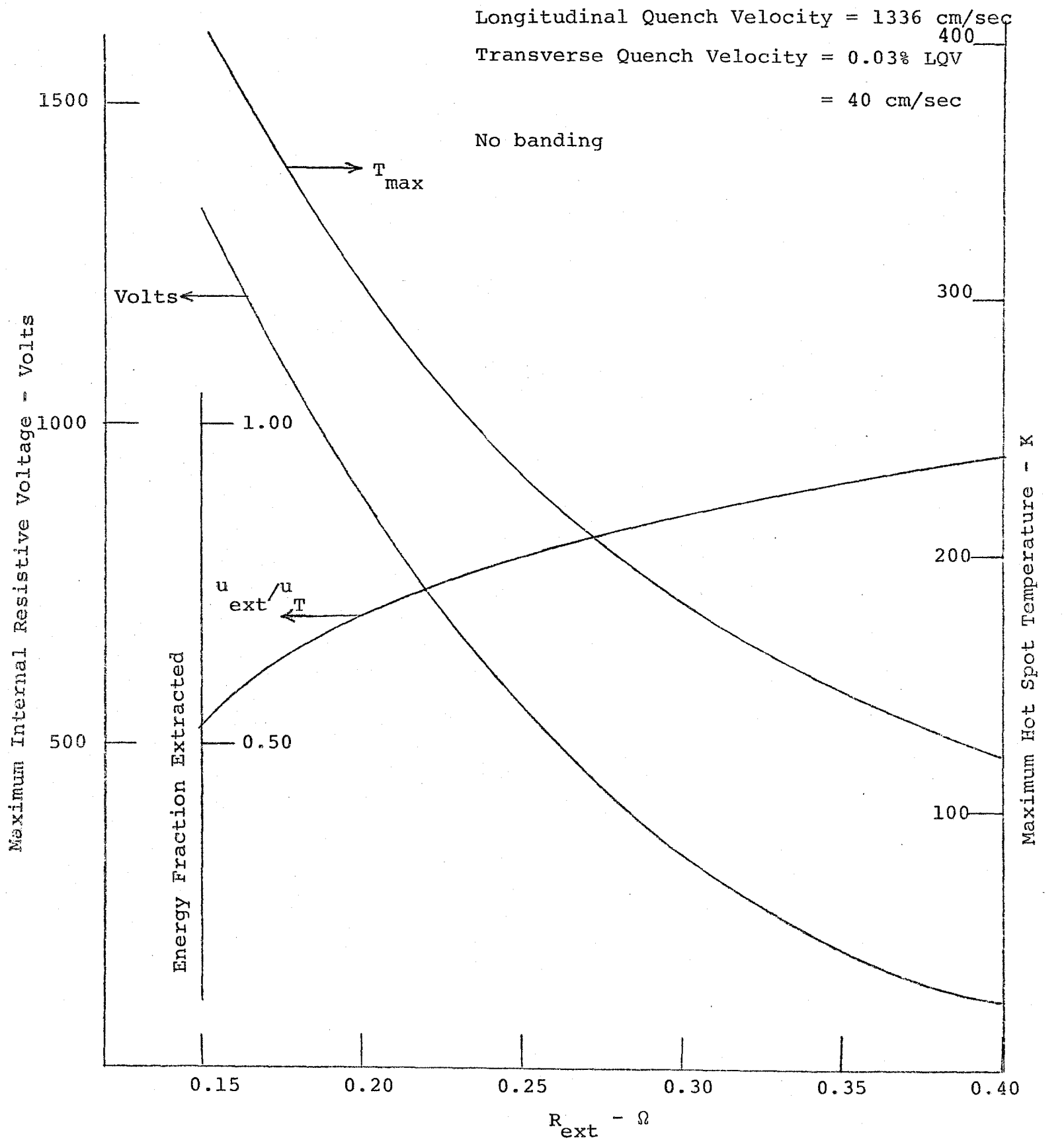

FIG. II-6

QUENCH CHARACTERISTICS vs. EXTERNAL RESISTANCE

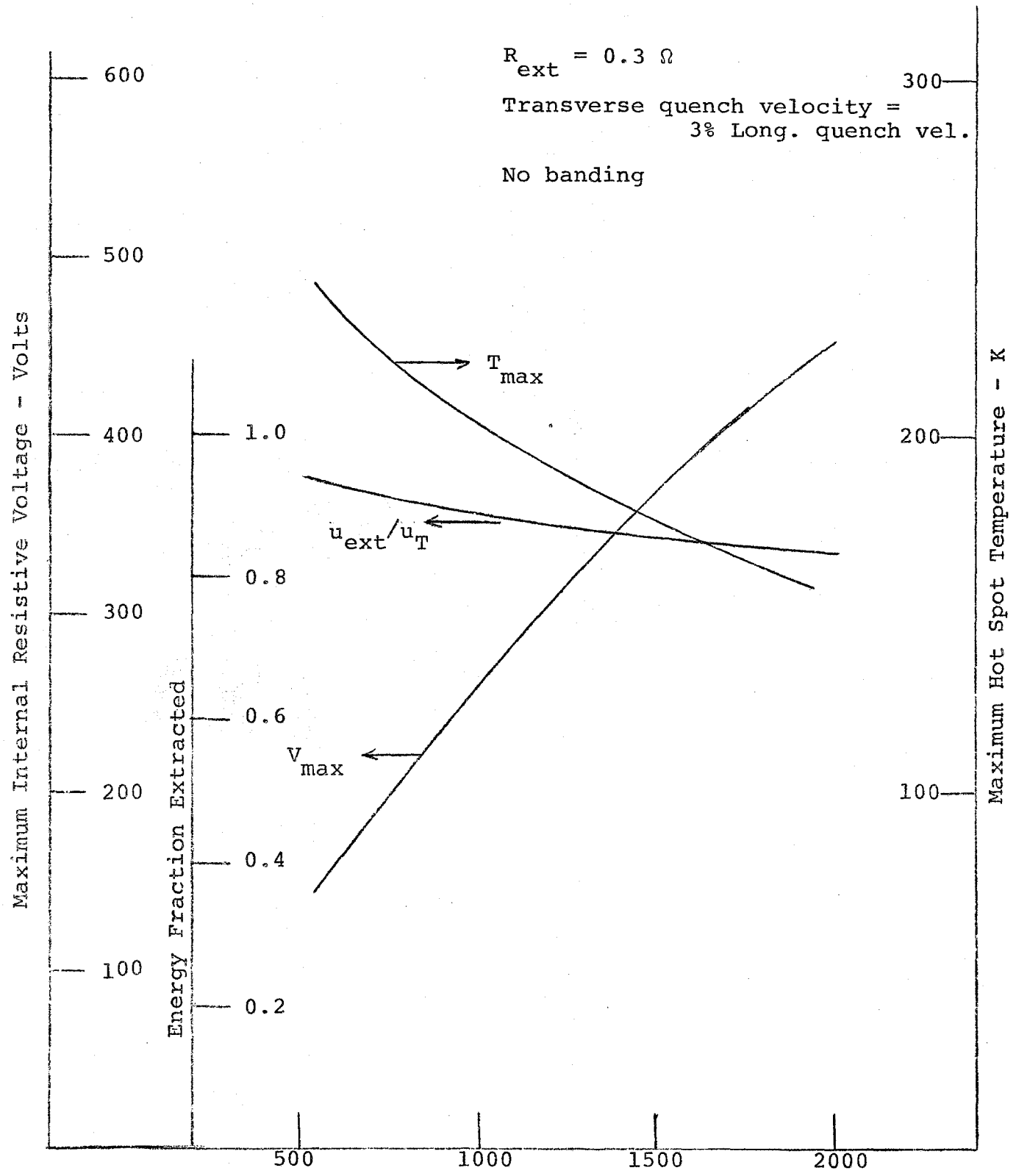

FIG. II-7

QUENCH CHARACTERISTICS vs. LONGITUDINAL QUENCH VELOCITY

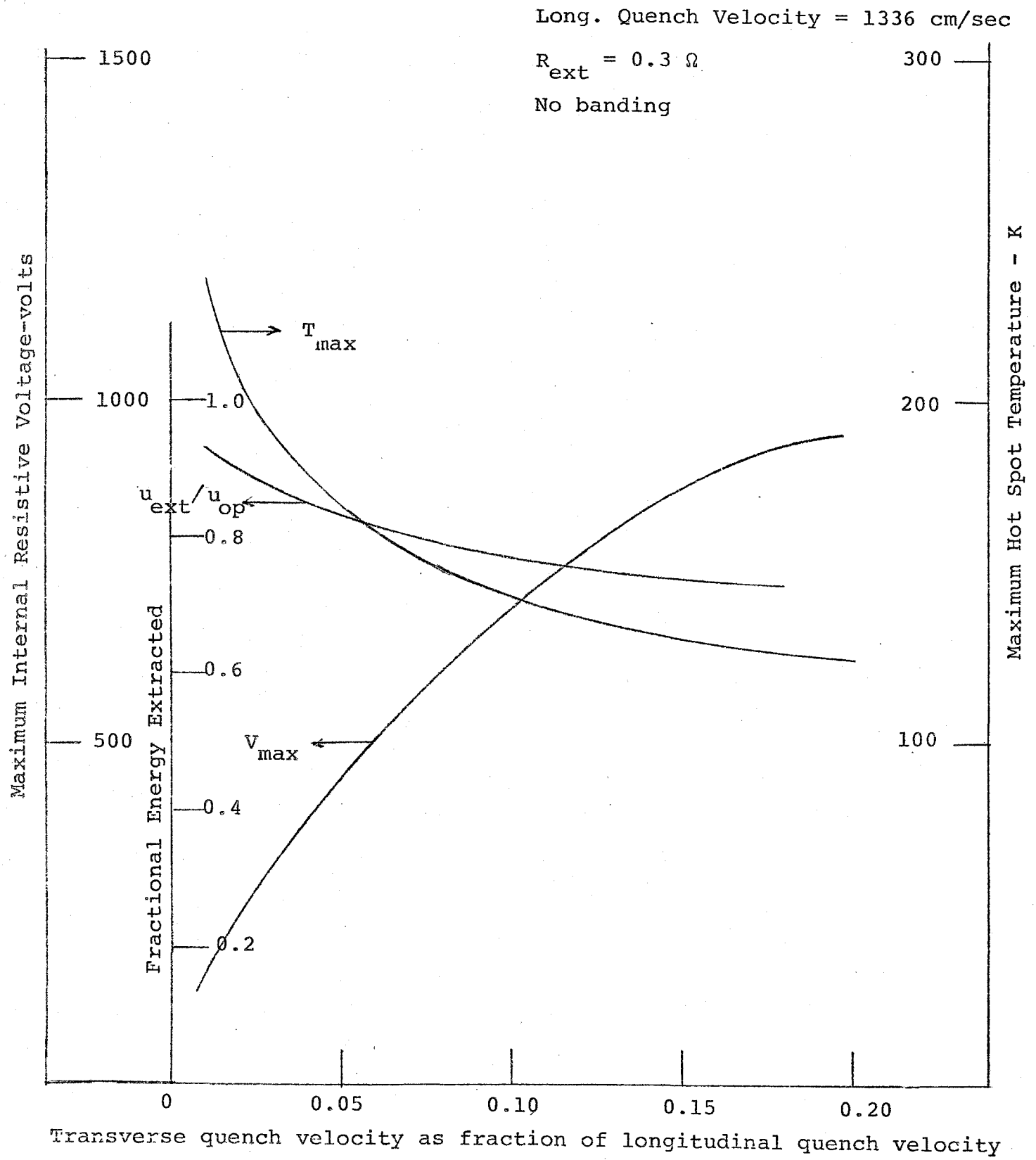

FIG. II-8

QUENCH CHARACTERISTICS vs. TRANSVERSE QUENCH VELOCITY

TABLE II-3

CURRENT SHARING IN HIGH-PURITY ALUMINUM

With I_0 = 5000 A, $R = 0.10\ \Omega$, u = 28 MJ, V_0 = 1000 cm/sec,

$V_\perp = 0.024\ V_0$, $I_{Al} = I_0(1-e^{-t/\tau})$, $\tau = \frac{4\mu_0 w^2}{\pi^2 \rho}$, no banding.

Current Sharing Time Constant	0.0 sec	0.35 sec ≈ B=2T	1.0 sec ≈ B=0T
Max. hot spot temperature	206 K	218 K	278 K
Decay time constant	7.4 sec	6.3 sec	4.9 sec
Max. internal resistive voltage	1335 V	1387 V	1642 V
Max. internal unbalance voltage	781 V	899 V	1185 V
Fractional energy extracted	43%	35%	27%

TABLE II-4

QUENCH CHARACTERISTICS OF INTEGRAL CONDUCTOR/STRUCTURE COIL DESIGN

With I = 5000 A, U = 28 MJ, V_o = 1000 cm/sec, R = 0.1Ω

	With Integral Al Banding ($\rho = \infty$)	Without Integral Banding
Discharge Time Constant	15 sec	7.4 sec
Maximum Hot Spot Temperature	128 K	206 K
Maximum Internal Resistive Voltage	300 V	1335 V
Maximum Internal Unbalance Voltage	57 V	781 V

One must interpret the results obtained from QUENCH with caution, but nevertheless the conductor/coil design proposed here appears to be safe against burn out and arc down during a quench. Additional work is required to reduce the uncertainties in the quench analysis.

REFERENCES

1. P. Genevy, et al., "Conductor for a 'Transparent' Solenoid for PETRA, Bratislava, 1977, Saclay Report STIPE/77-51.
2. P. Genevy, op. cit.
3. P. Turowski, "Results of Quench Propagation in 'CELLO' Conductor", Bratislava, 1977.
4. M. Wilson, et al., "Computer Simulation of the Quenching of a Superconducting Magnet, RHEL/M/151.
5. H.R. Segal, "Reinforced Aluminum as a Superconducting Magnet Stabilizer", IEEE Trans. on Mag, Vol. Mag-13, P-109, 1977.
6. S.H. Kim and S.T. Wang, "Measurements of Mechanical and Electrical Properties of High Purity Aluminum, unpublished.
7. P. Genevy, up. cit.
8. P. Komarek and H. DesPortes, "Magnetic Field System for PETRA Experiment (Proposal)" Saclay Report Stipe/76-52, 1976.
9. M. Wilson, op. cit.
10. P. Turowski, "Investigation of the Propagation Velocity of a Normal-Conducting Zone in Technical Superconductors", Cryogenics, 18, 515 (1978).
11. P. Genevy, op. cit.

III. YOKE DESIGN

A. End Cap Calorimeter

The end cap calorimeter is shown in Figures III-1, I-2a, b. It consists of a stationary portion and a plug. The plug is laminated with 2" steel plates separated by 1/2" air gaps, all surrounded by a 1/2" thick steel shell. A hole 2 feet in diameter along the axis accommodates both beam line pipes. The plug is split in half along the vertical axis for easy removal. The stationary part of the axial calorimeter is also made of 2" steel-1/2" air laminations terminated all around the axis by a concave recess of 1/2" steel into which the plug fits.

B. Magnetic Field Calculations in Two and Three Dimensions

Two Dimensional Calculations: The magnetic fields and the forces on the coil have been calculated for the colliding beam detector using the program TRIM.[1] TRIM makes calculations in two dimensions and assumes cylindrical symmetry. Many different coil-iron geometries have been calculated to find an optimum solution where the axial force on the coil is manageable and the magnetic field outside the coil is low enough to permit the use of photo-multiplier tubes. For the best solution two iron plates are inserted into the coil about 4 inches. The flux is returned through the 2" iron plates at the ends of the coil. Since cylindrical symmetry is assumed with TRIM, output is given as

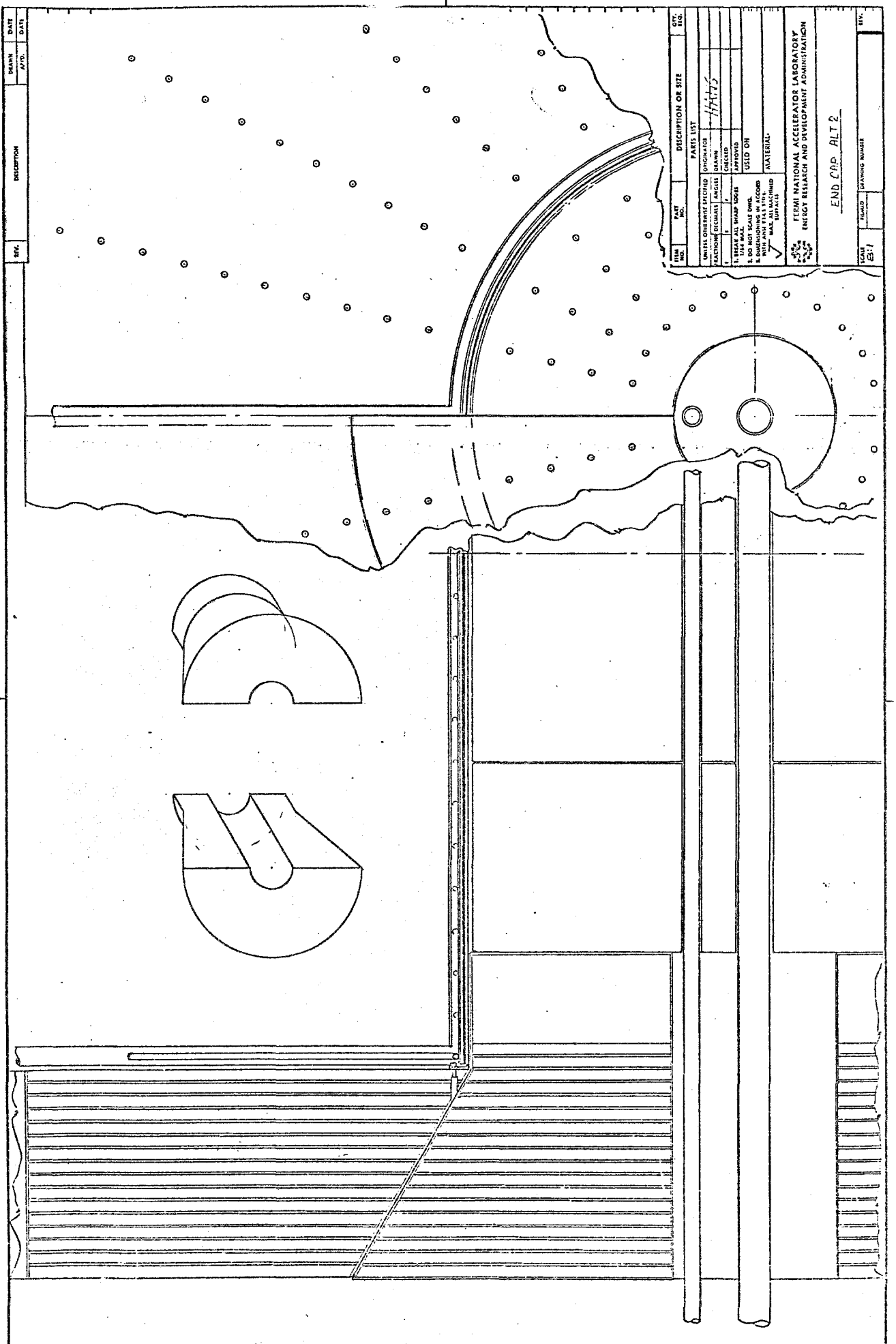

FIG. III-1 End Cap Calorimeter

the flux, $\phi = \vec{A} \cdot \vec{r}$ where $\vec{A}$ is the vector potential and $\vec{r}$ is the radius vector. A plot of the flux is given in Figure III-2. From this plot, it is clear that the iron is completely saturated near the coil and that the magnetic field is very small outside the coil and very uniform inside. In Figure III-3 the axial and radial components of the magnetic field at various locations are shown. About 8" from the flux return and the coil, the magnetic field has dropped to the vicinity of a few hundred gauss. Near the median plane of the coil the magnetic field is even smaller. Both axial and radial forces are shown on a logarithmic plot in Figure III-4. The axial force is negative, indicating that the coil is under compression. The radial force is outward. Both forces are manageable without excessive structure.

To increase the flexibility of the detector, the end plug described in III-A can be removed and the space used for other instrumentation, provided that the fringe fields and forces on the coil do not become too large. To check this, TRIM was run with the end plug removed. The end plug is surrounded by two 1/2" thick conical steel shells, one mobile and one stationary. This was modeled in TRIM by one 1" shell which was removed with the end plug, thus the results from TRIM are likely to be worse than they would be with 1/2" thick steel left in place.

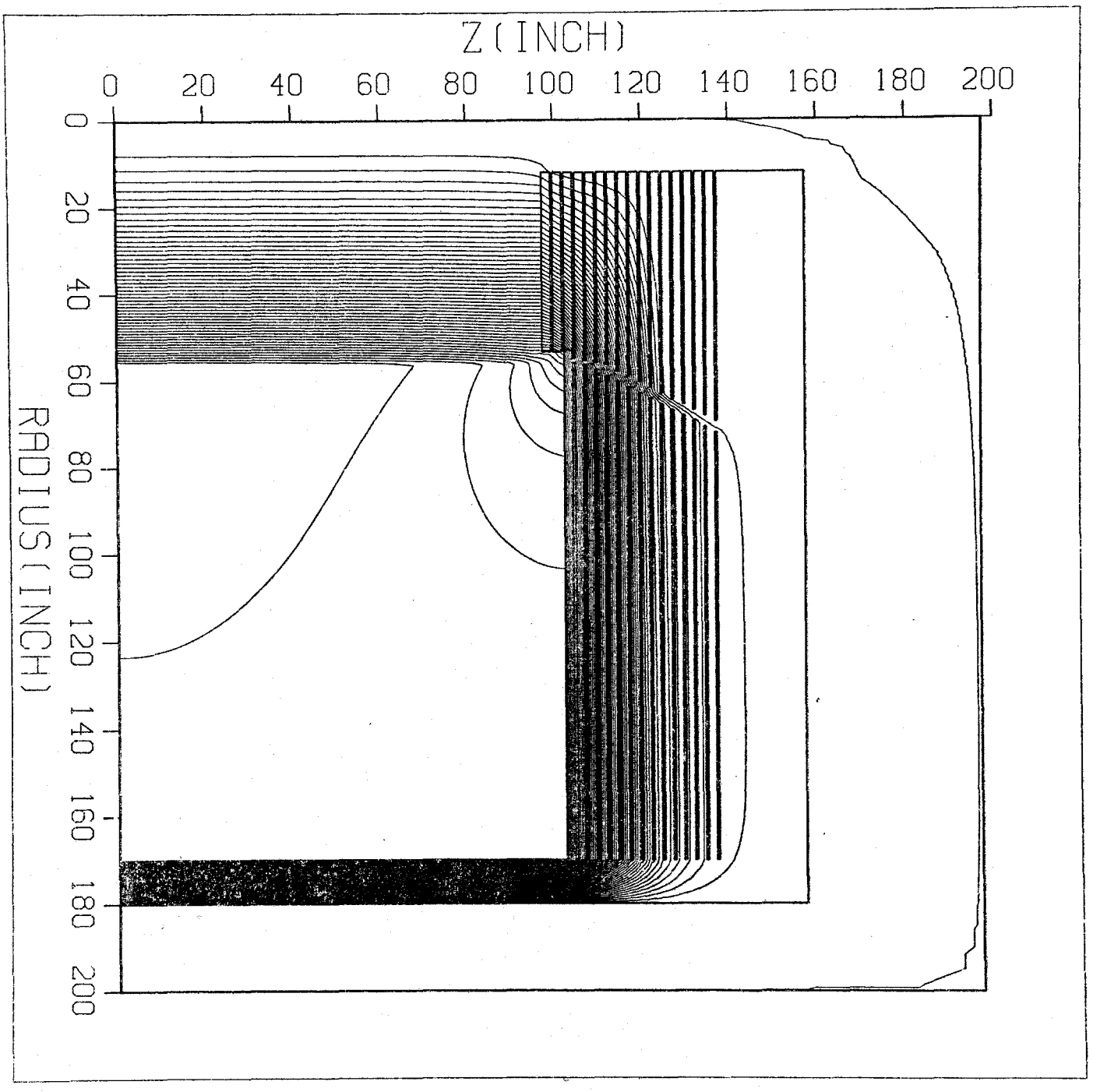

FIG. III-2

Flux plot - Plug in

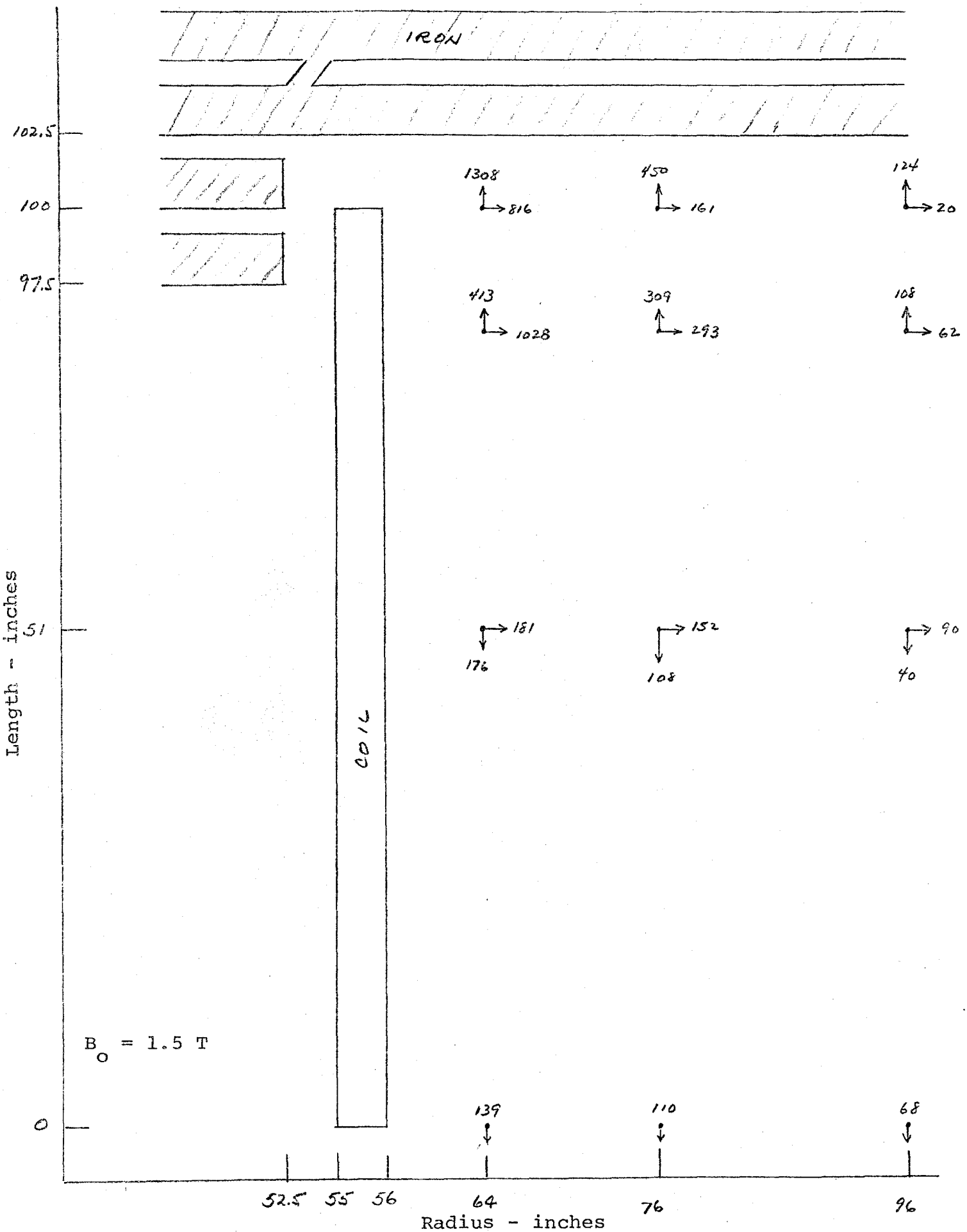

FIG. III-3 Fringe Field in Air - End Plug In

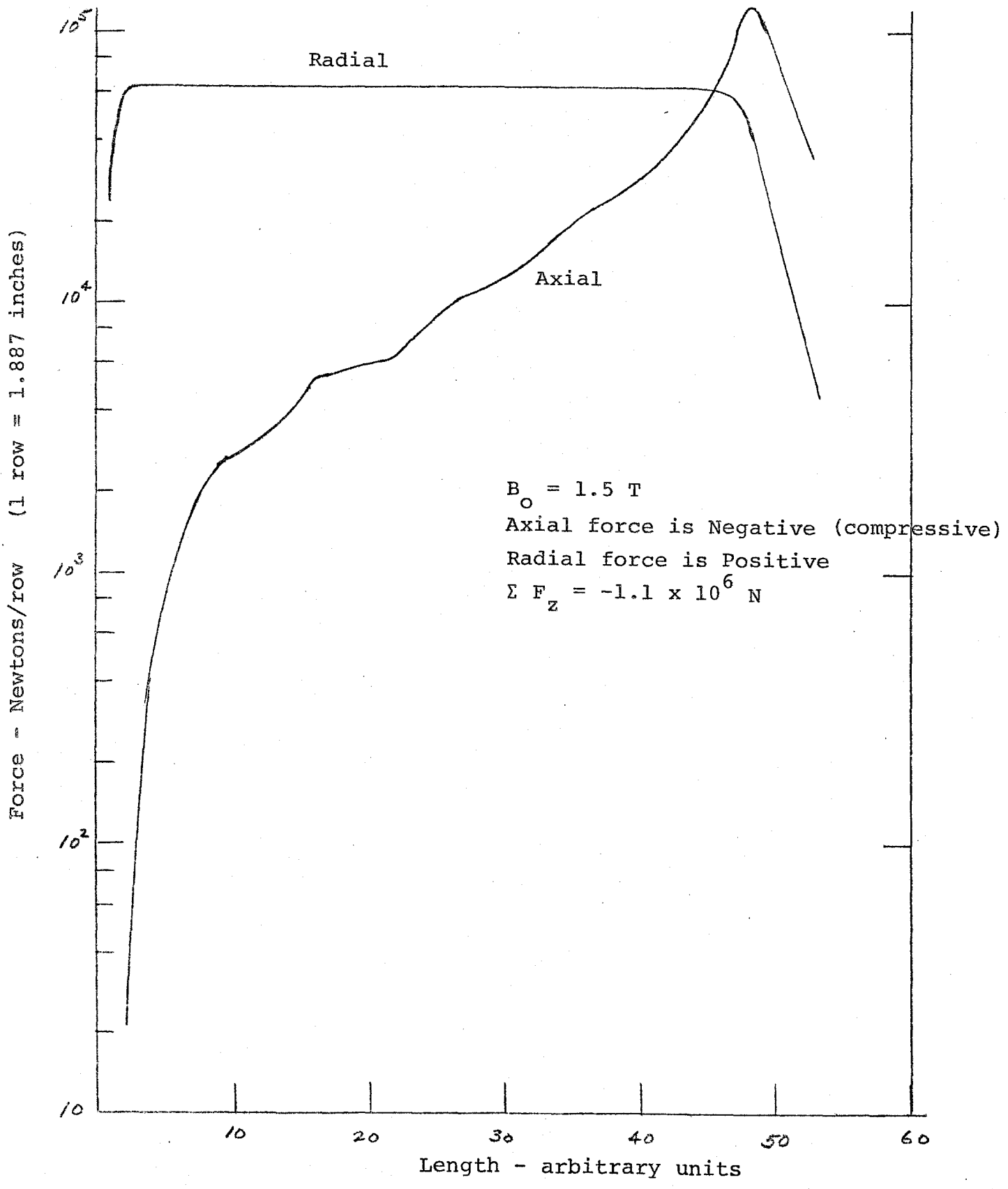

FIG. III-4 Axial and Radial Forces - Plug In.

The central field of the solenoid was reduced from 1.5T to 1.0T. The results are shown in Figures III-5, 6, and 7. The fringe fields are somewhat higher than with the end plug in place, but photomultiplier tubes could still be used in at least part of the space. The forces on the coil are of the same magnitude as before.

Three Dimensional Calculations: The iron plates, yoke, and return legs are not axially symetric, but rather are symetric about a 45° reflection. It was felt desirable to do a three dimensional calculation using GFUN3D[2,3] to study the azimuthal variation of the field. A coil of inner radius 140cm, thickness 1cm, and height 492cm with current density 14,000A/cm^2 was located 5.08 cm (2") vertically and 4.80 cm (1-7/8") horizontally from the iron. The calculated field is shown in Figure III-8 and in Table III-1. Note that the field is almost independent of the azimuth except very near the iron. Although GFUN3D is the only known three dimensional magnetostatic program incorporating iron of variable permeability, the calculation is difficult because only 200 iron elements are available to model the complex, laminated iron structure. The results given here are not completely converged due to limited availability of computer time. Even with these limitations, the GFUN results show that the field is essentially independent of azimuth in the regions of interest and that there is uncertainty in the value of the fringe field outside the coil.

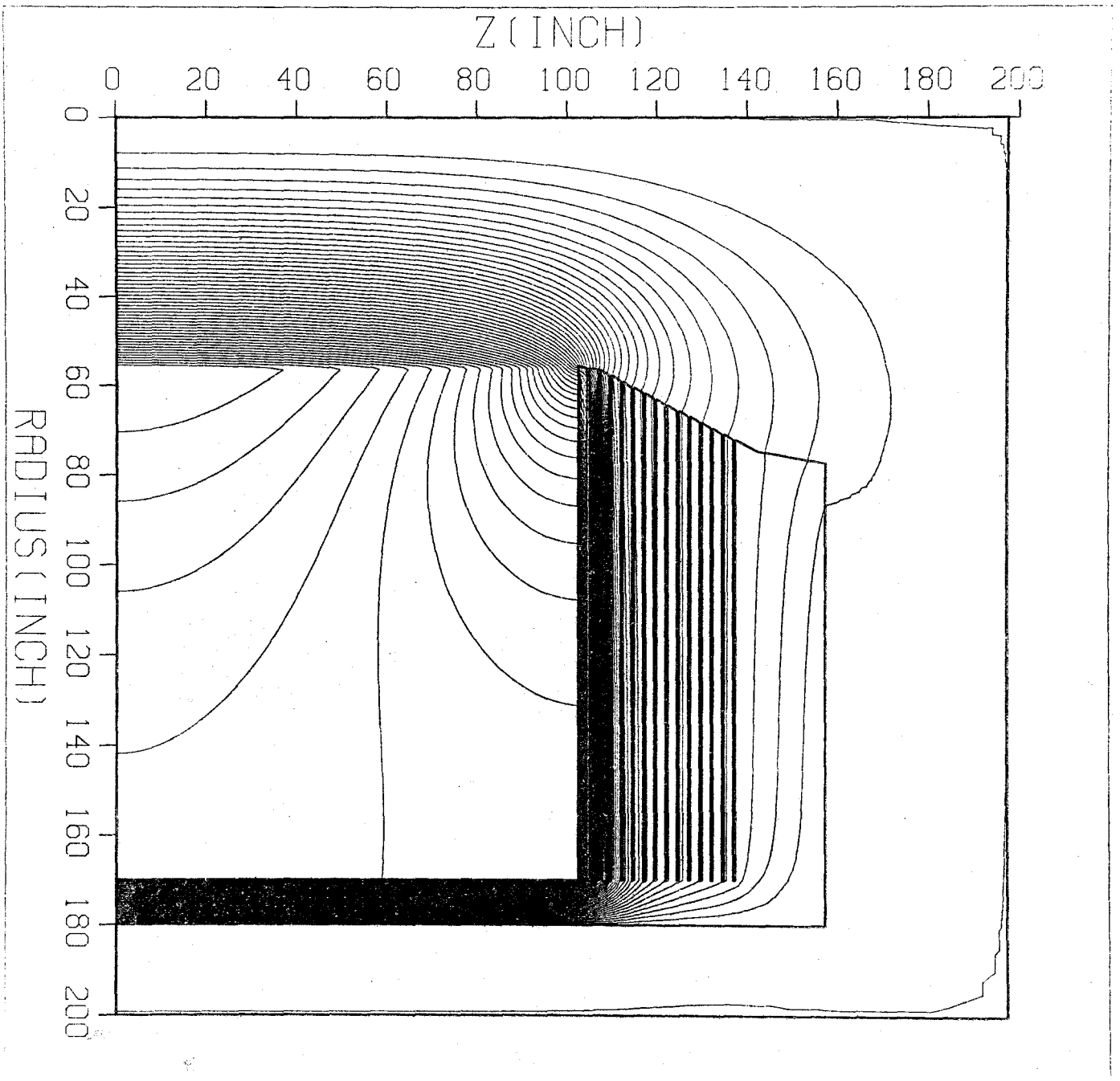

FIG. III-5

Flux Plot - Plug Out

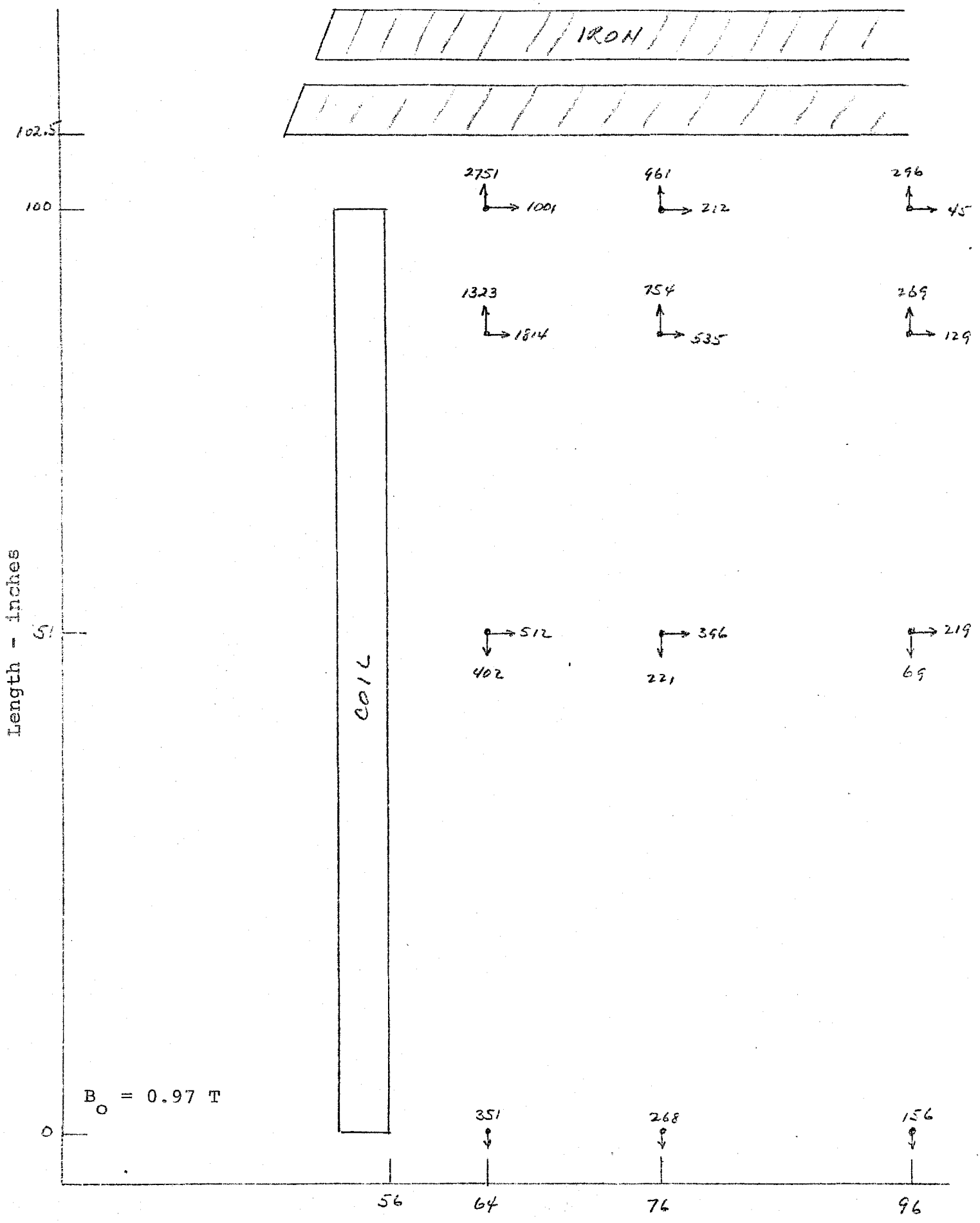

FIG. III-6 Fring Field in Air - Plug Out

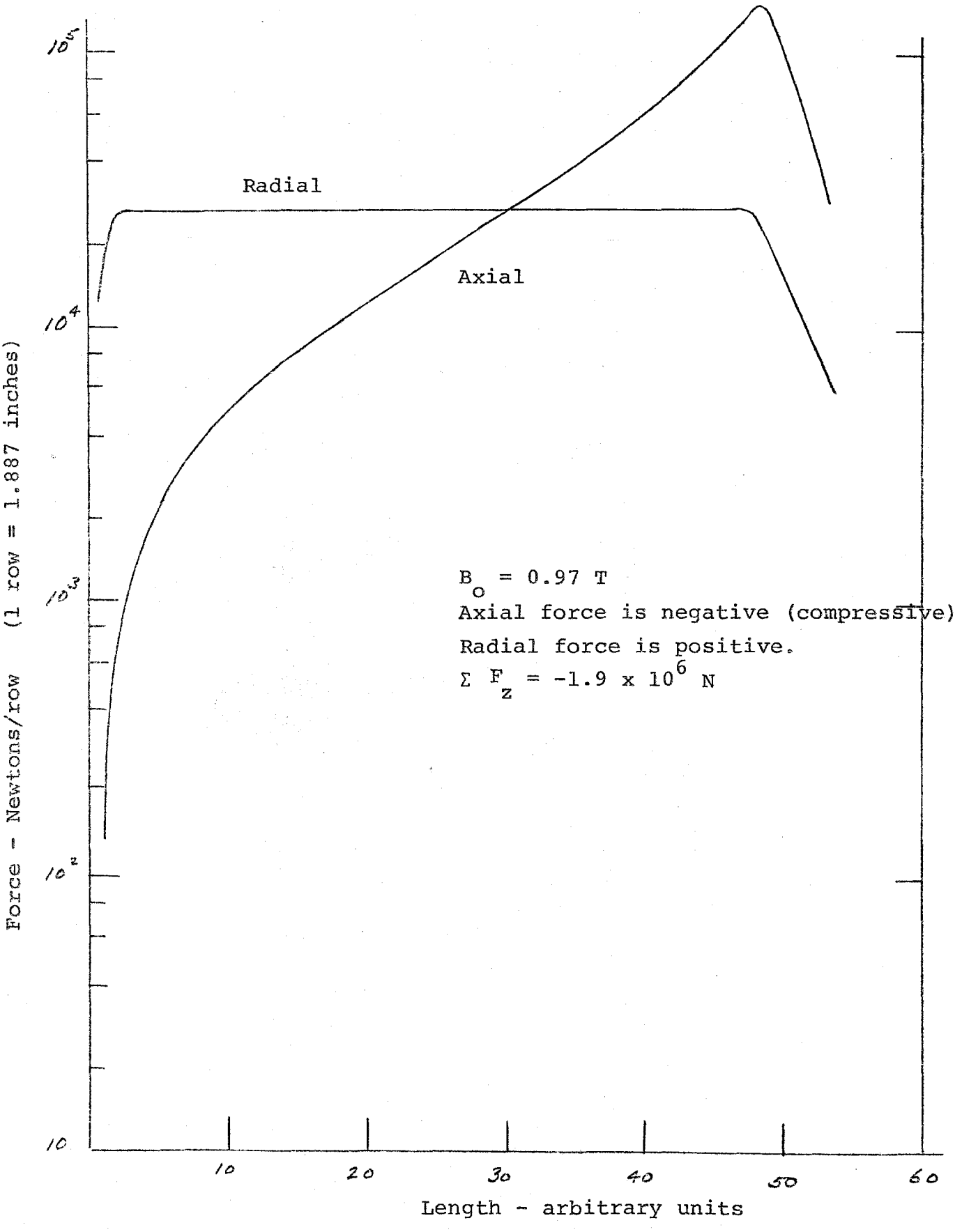

FIG. III-7 Axial and radial forces - Plug Out

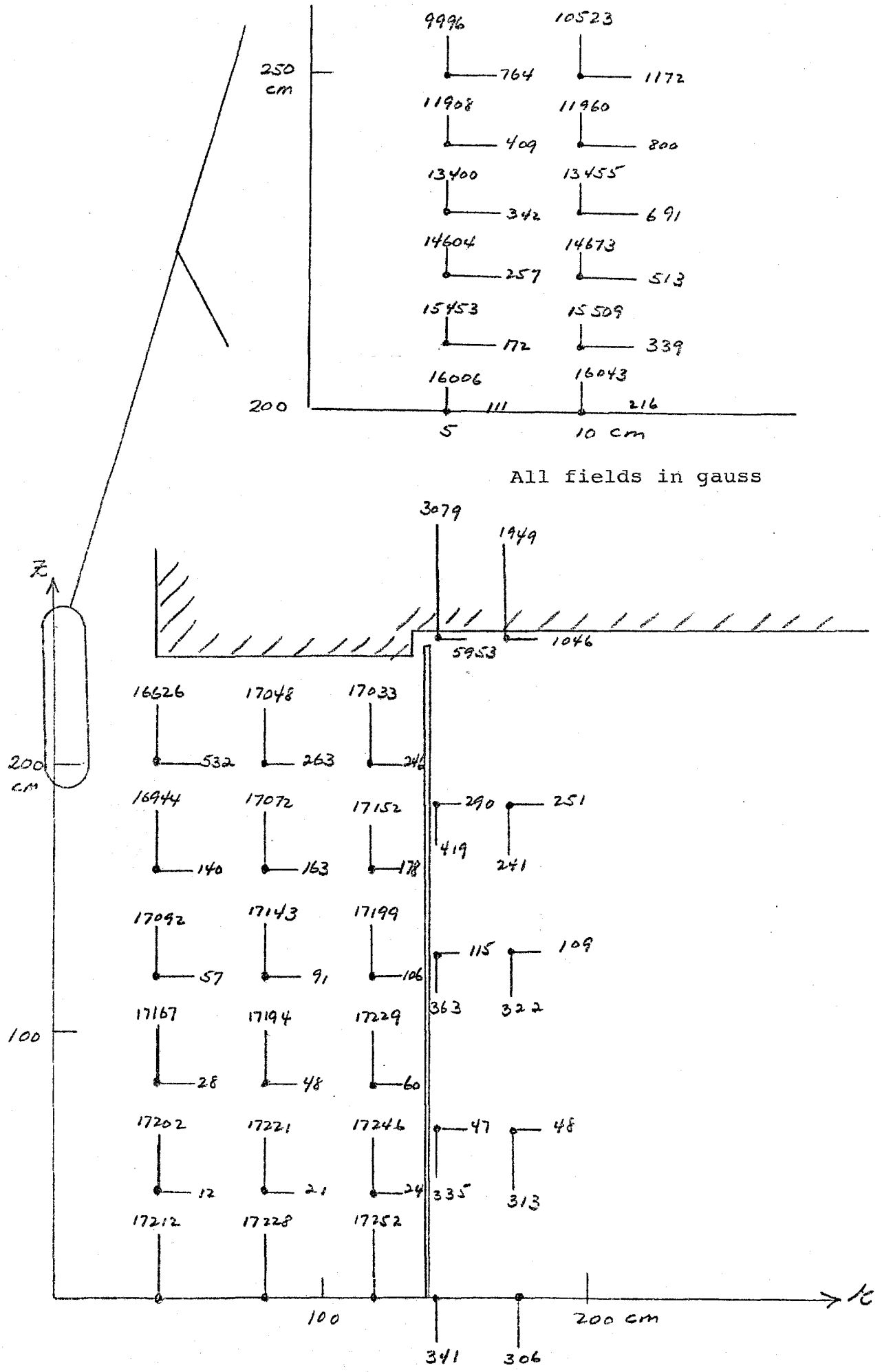

FIG. III-8 GFUN RESULTS

TABLE III-1

Results of GFUN Calculation

H_Z (Gauss) vs. Θ , Z, O

Inside Coil

r(cm)	Z(cm)	0°	15°	30°	45°	60°	75°	90°
40	0	17212	17212	17212	17212	17212	17212	17212
	40	17202	17202	17202	17202	17202	17202	17202
	80	17166	17166	17167	17167	17167	17167	17167
	120	17091	17091	17092	17092	17093	17093	17093
	160	16940	16940	16942	16944	16947	16948	16949
	200	16608	16611	16618	16626	16635	16642	16644
80	0		17229	17229	17228	17227	17227	
	40		17221	17221	17221	17220	17220	
	80		17193	17193	17194	17193	17193	
	120		17139	17141	17143	17144	17144	
	160		17058	17065	17072	17076	17078	
	200		17005	17025	17048	17064	17075	
120	0		17254	17253	17252	17250	17249	
	40		17247	17247	17246	17245	17243	
	80		17227	17228	17229	17227	17225	
	120		17191	17195	17199	17198	17194	
	160		17126	17140	17152	17151	17144	
	200		16968	17007	17033	17041	17032	
				Outside Coil				
142	0	- 341	- 339	- 340	- 341	- 344	- 347	- 349
	62	- 337	- 336	- 335	- 335	- 338	- 341	- 343
	124	- 379	- 376	- 368	- 363	- 367	- 374	- 378
	186	- 504	- 494	- 449	- 419	- 435	- 470	- 479
	248	4433	3433	4187	3079	3150	2844	5004

r	Z	0°	15°	30°	45°	60°	75°	90°
172	0		- 304	- 304	- 306	- 311	- 315	
	62		- 312	- 311	- 313	- 317	- 322	
	124		- 336	- 327	- 322	- 330	- 341	
	186		- 363	- 298	- 241	- 288	- 354	
	248		30	1566	1949	2416	221	

Hole Region

		H_z (Gauss)			H_r (Gauss)		
r	Z	15°	45°	75°	15°	45°	75°
5	200	16006	16006	16007	107	110	113
	210	15453	15453	15453	167	172	176
	220	14603	14604	14604	251	257	262
	230	13401	13400	13398	338	342	344
	240	11918	11908	11896	421	409	394
	250	10069	9996	9998	863	764	597
10	200	16042	16043	16044	210	216	223
	210	15508	15509	15510	331	339	348
	220	14672	14673	14673	501	513	523
	230	13459	13455	13449	680	691	699
	240	11986	11960	11918	796	800	775
	250	10611	10523	10185	1174	1172	937

Comparison of Calculations: The two programs used to calculate the magnetic field, TRIM and GFUN, both have disadvantages. TRIM can not model in three dimensions, GFUN can not model the complex geometry due to limitations in the number of elements available. To compare results from the two programs, TRIM was run using the simplified geometry of GFUN, and with identical parameters. The results are shown in Table III-2. The TRIM value is compared with the range of GFUN values obtained at different azimuths. Fields are not given for the same points in the two programs; hence, in some cases the values given are approximate. Inside the coil the results from TRIM are approximately 3% higher than those from GFUN. Just outside the coil ($r = 142$ cm) the fields are decreasing so rapidly that it is difficult to make a realistic comparison. The fringe fields outside the coil are generally lower from TRIM than from GFUN. Within the hole region the results from TRIM are slightly higher for H_z. The radial components of the field in the hole appear to peak at different values of z in the two programs.

TABLE III-2

TM-826
2750.000

Comparison of TRIM and GFUN Results

Inside Coil

r (cm)	z (cm)	H_z (gauss) GFUN min	GFUN max	TRIM
40	0	17212	17212	17720
	40	17202	17202	17250
	80	17166	17167	17830
	120	17091	17093	17200
	160	16940	16949	17180
	200	16608	16644	17450
80	0	17227	17229	17636
	40	17220	17221	17410
	80	17193	17194	17690
	120	17139	17144	17400
	160	17058	17078	17420
	200	17005	17075	17850
120	0	17249	17254	17617
	40	17243	17247	17468
	80	17225	17229	17660
	120	17191	17199	17470
	160	17126	17152	17490
	200	16968	17041	17740

Outside Coil

142	0	-339	-349	500
	62	-335	-343	1000
	124	-363	-379	445
	186	-419	-504	436
	248	3844	5004	1666
172	0	-304	-315	-20
	62	-311	-322	-20
	124	-322	-341	-20
	186	-241	-363	-42
	248	30	2416	180

r(cm)	z(cm)	H_z(Gauss) GFUN min	GFUN max	TRIM	H_R(Gauss) GFUN min	GFUN max	TRIM
5	200	16006	16007	16500	107	113	55
	210	15453	15453	15924	167	176	390
	220	14603	14604	14940	251	262	144
	230	13398	13401	13530	338	344	875
	240	11896	11918	12200	394	421	530
	250	9886	10069	11000	597	863	460
10	200	16042	16044	16600	210	223	166
	210	15508	15510	16000	331	348	555
	220	14672	14673	15060	501	523	413
	230	13449	13459	13500	680	699	1200
	240	11918	11986	12100	775	800	900
	250	10185	10611	10600	37	1174	650

C. Forces on Yoke Components - Laminated End Cap Plates, Removeable End Cap Plug

The magnetic field in the stationary part of the axial calorimeter has no appreciable axial component to deform the plates, see Figure III-2. The axial force on the plug is supported by vertical beams extending to the stationary part, see Figure I-2a, b. The axial pressure on the first plate, calculated from the TRIM output, is shown in Figure III-9. Each 2" plate in the plug is welded along its half circumference to the 1/2" steel cone shell. Preliminary stress analysis indicates that the design is safe with 2" steel plates, but it is not possible to use 3/4" plates for a finer calorimeter.

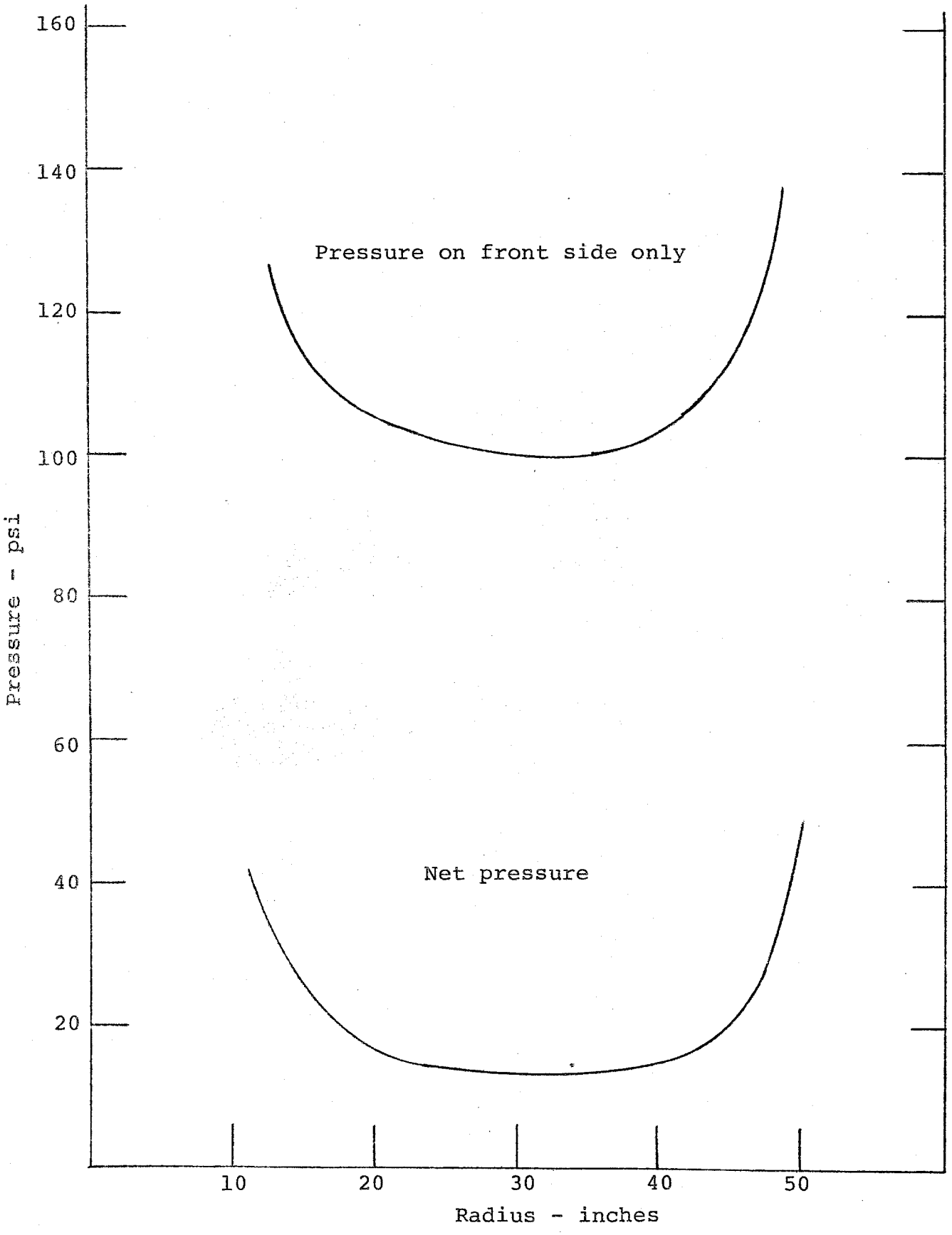

FIG. III-9

PRESSURE ON FIRST PLATE IN END CONE

D. Decentering Forces

Axial Decentering

When the coil is centrally positioned, the forces F_0 on it are equal and opposite (Figure III-10a). To calculate the decentering force F_D, the coil should be displaced slightly, and the decentering force is then given by the difference between the two forces, $F_1 - F_2$ (Figure III-10b). The program TRIM uses only half the coil and has an axis of symmetry through the center of the coil, so the coil can not be displaced. There are insufficient mesh points available for the whole coil to be used without the geometry being oversimplified.

To approximate the decentering force, TRIM was run twice, with the coil half an inch longer than the nominal value giving force F_1' and half an inch shorter giving force F_2' (Figure III-10c, d). This was repeated with displacements of one inch.

The difference between the two forces is very small compared with either force, and is expected to occur mainly at the end of the coil, which is most affected by alterations in the axial gap. When the two forces were plotted as functions of Z, it could be seen that slight oscillations in the solutions along the coil were producing differences in the integrated forces. There also appeared to be a real difference in the forces at the end of the coil. To eliminate the spurious differences along the coil and concentrate on the real differences at the end of the coil, the forces were integrated only from 87" to the end of the coil. These

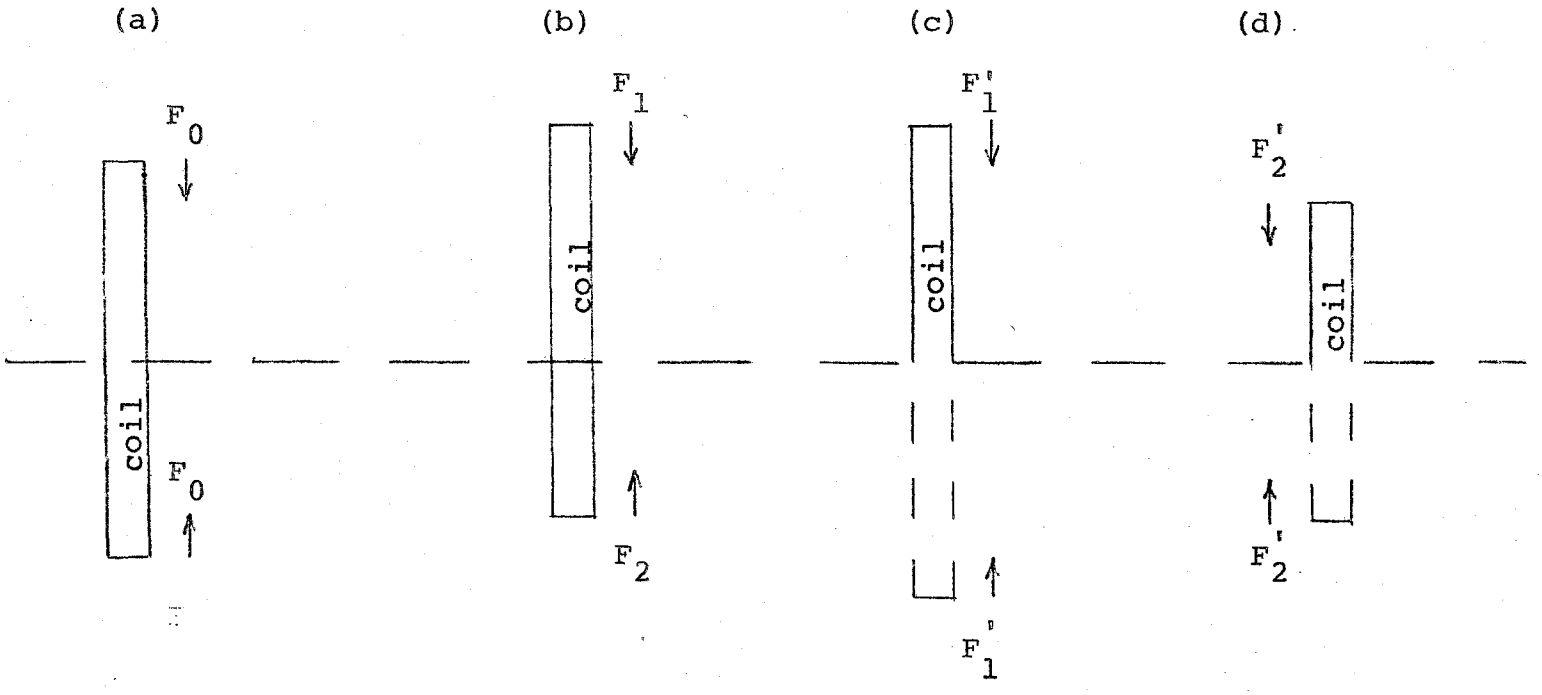

FIG. III-10

COIL GEOMETRY FOR CALCULATION OF AXIAL DECENTERING FORCE

forces are shown in Table III-3. The results show that the axial decentering force is very small. This is to be expected since the flux plot (Figure III-2) shows that there is little divergence of the magnetic field at the end of the coil. The force is also strongly non-linear (2.4×10^2 N/cm for 1/2" displacement, 2.8×10^3 N/cm for 1" displacement).

Radial Decentering

The radial decentering force was approximated in the same way by increasing and decreasing the radius of the coil by 1/2". It was not repeated with a displacement of 1" since this would have required extensive alteration of the mesh. The decentering force F_D is given by:

$$F_D = 2[F_\theta \ (r + \Delta r) - F_\theta \ (r - \Delta r)]$$

and is shown in Table III-2 to be 1.6×10^5 N/cm. This is high, but experience has shown that the radial distance between the coil and the re-entrant steel plates is critical.

TABLE III-3

Decentering Forces in Coil

Axial Decentering Force:

ΔZ	$\lvert F_1' \rvert$ (N)	$\lvert F_2' \rvert$ (N)	$\lvert F_1' - F_2' \rvert$ (N)	F_D (N/cm)	F_D (lb/in)
1/2"	6.712×10^5	6.715×10^5	3×10^2	2.4×10^2	1.37×10^2
1"	6.700×10^5	6.770×10^5	7×10^3	2.8×10^3	1.60×10^3

Radial Decentering Force:

Δr	$F_1' = \lvert F_0 (r + \Delta r) \rvert$ (N)	$F_2' = \lvert F_0 (r - \Delta r) \rvert$ (N)	$\lvert F_1' - F_2' \rvert$ (N)	F_D (N/cm)	F_D (lb/in)
1/2"	3.90×10^6	3.19×10^6	10^5	1.6×10^5	9.1×10^4

E. Interaction of Yoke and Coil Upon Fast Coil Discharge

A thin solenoid without iron exerts considerable compressive axial force upon itself. An iron-free solenoid was modeled by a coil of 280cm inside diameter, 1cm thickness, 492cm high, with a current density 14,000A/cm^2. The axial compressive force at the midplane was calculated to be 1.505 x 10^6 lb. (6.69 x 10^6N). One of the functions of the iron is to exert a tensile force which cancels most of the axial compressive force in the coil. In the GFUN calculation with iron, the compressive force on the midplane due to both coil and iron was 0.388 x 10^6 lb. (1.73 x 10^6N), corresponding to a tensile force from the iron of 1.117 x 10^6 lb. (4.97 x 10^6N).

It could happen in the event of a quench that the field from the coil could die out faster than eddy currents would permit the field from the iron to die out. A possible consequence is that at sometime during the decay, the coil could experience a net axial tension. In the absence of information about the decay time of the field from the iron, we make the pessimistic estimate that the field from the iron does not change while the field from the coil decays. We wish to find the maximum axial tension during the decay. Let $X = I/I_o$, the ratio of the current at a given time to the initial value. The force from the iron is then proportional to X, while the force from the coil on itself is proportional to X^2. We write:

$$F = X F_I + X^2 F_C \qquad (2)$$

when F_I and F_c represent the initial value of the axial forces from the iron and coil respectively.

We maximize the magnitude of F when:

$$X = -F_I/2F_c; \tag{3}$$

in which case:

$$F_{max} = -X^2F_c = -F_I{}^2/4F_c. \tag{4}$$

Using the above values for F_c and F_I, we find that the maximum tensile force occurs at X = 0.37 and has the magnitude 0.207×10^6 lb. (0.921×10^6N). If instead, the iron is designed to completely cancel the compressive axial force from the coil, then $F_I = -F_c$; X = -0.5, and the maximum tensile force is 0.376×10^6 lb. (1.67×10^6N). The coil must be constructed to withstand axial tension of this amount, in addition to a steady state compression of about the same value ($.388 \times 10^6$ lb = 1.73×10^6N).

REFERENCES

1. R. Lari, J.K. Wilhelm, Computer Program Trim for Magnet Design, ANL report (unpublished).
2. M.J. Newman, C.W. Trowbridge, and L.R. Turner, "GFUN: An Interactive Program as an Aid to Magnet Design", Proc. Fourth International Conference on Magnet Technology, Brookhaven pp. 617 - 626 (1972).
3. A.G. Armstrong, et al., "GFUN3D User Guide", Rutherford Laboratory, RL-76-029/A (November, 1976).

IV. CRYOSTAT DESIGN AND FABRICATION

A. General Features

Figure IV-1 shows the general features of the coil, support system, and cryostat vessels. The materials used are primarily aluminum with an epoxy-fiberglass support structure to ambient temperature and possibly an epoxy-fiberglass coil bobbin. The cryostat was designed to allow the coil to be located 2 inches from the iron end cap. Depending on the refrigerator used, the radiation shields may be considered as optional.

B. Coil and Helium Vessel

Several coil designs were discussed in Section II and details of the tube cooling circuit given in Section V. The combination of coil bobbin and banding support the steady-state axial compression and possible tension during quench or fast discharge. End clamps serve to maintain the axial preload in the conductor and anchor the banding. Liquid helium is contained only in the cooling tube, which is either longitudinal or spiral wound on the banding.

C. Support System

Axial stiffness to withstand axial decentering forces is provided by a stainless steel spoke system located from the longitudinal center of the coil to the inner vacuum vessel. The center location permits thermal contraction about a symmetric point, maintaining coil symmetry in the iron. Epoxy-fiberglass turn-buckles from the coil end flanges to the inner vacuum tank wall provide radial stiffness and support the

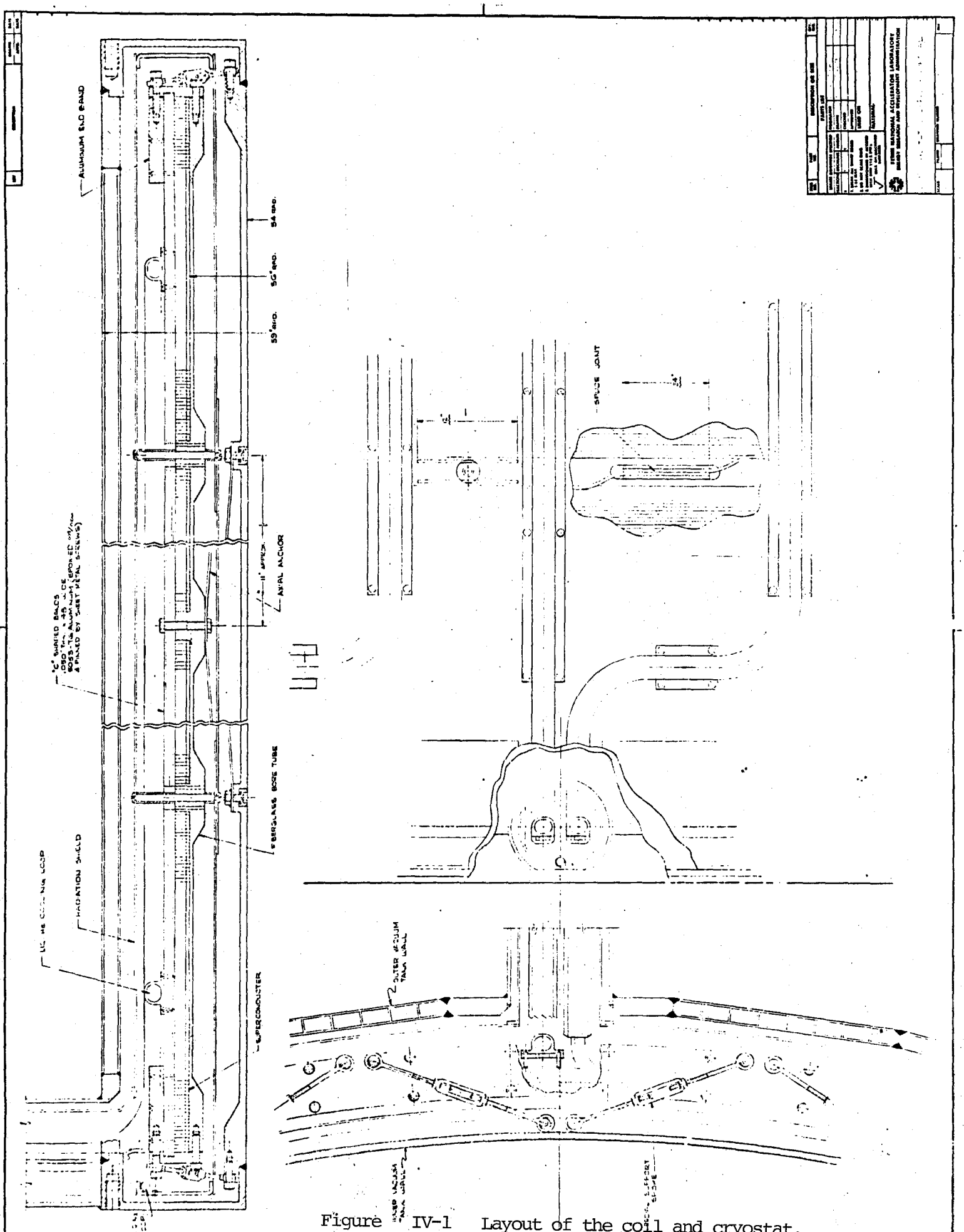

Figure IV-1 Layout of the coil and cryostat.

cold mass. The turnbuckles are set at angles so the coil remains centered during cooldown.

D. Radiation shields

The radiation shields are aluminum shields approximately 1/16" ($\sim$ 1.5mm) thick, supported either through the coil as shown or from the vacuum vessels. The shields are trace cooled with liquid nitrogen.

E. Vacuum Vessels

Two cylindrical vacuum shells are required for the cryostat. The inner shell is subject to steady-state internal pressure, and it also provides the axial stiffness for the decentering forces of the coil. A 1/4" (6.4mm) thick shell with a radiation length of .07λ will be adequate for this. Overpressure in the vacuum space causing a collapse load on the inner shell will be controlled with rupture disks.

The outer shell is designed for buckling external atmospheric pressure loading. Aluminum extrusions shown in Figure IV-2 welded lengthwise together to form a 46 sided polygon, provide an inexpensive, thin outer vacuum shell. The die for this particular extrusion is available to us. The average radiation length of the extrusion is 0.054λ , equivalent to 0.188" (4.8mm) aluminum sheet. Calculations (Appendix X-C) show that a vessel fabricated from this material, held circular at the ends and mid length, is adequate for the vacuum load with a safety factor of 1.9.

A 3/8" (9.5mm) thick rolled aluminum shell with four

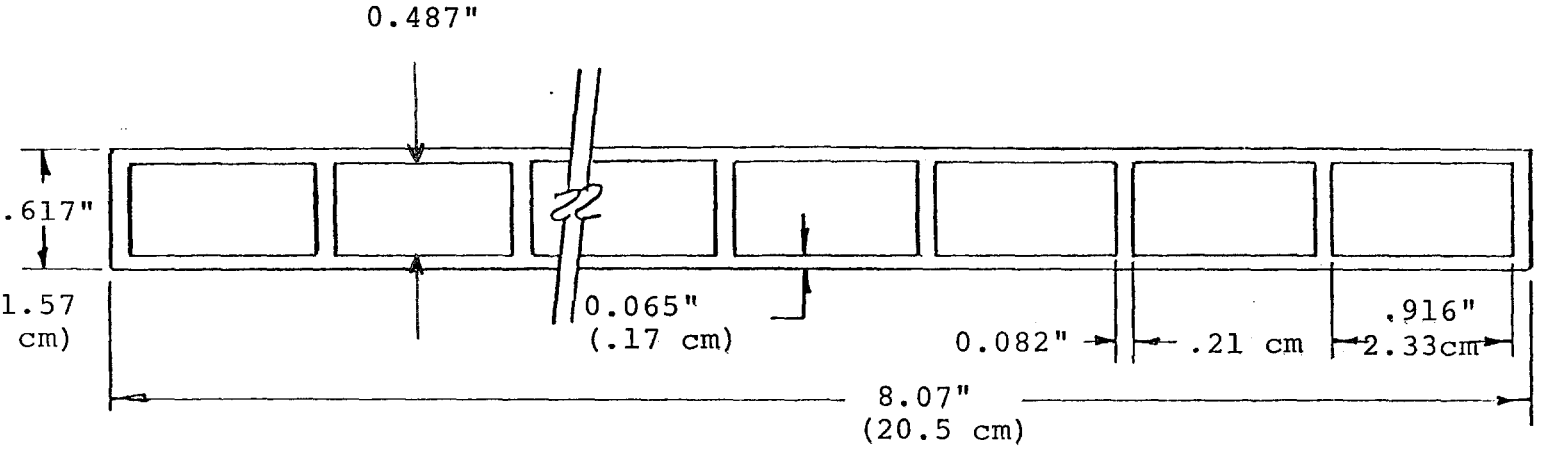

FIG. IV-2

ALUMINUM EXTRUSION USED FOR OUTER VACUUM VESSEL.

reinforcing ribs and a Kevlar epoxy filament wound shell were considered but do not appear as promising with regard to cost and radiation thickness.

F. Fabrication Procedure

A possible fabrication procedure for the coil and cryostat is given in Appendix X-D.

V. REFRIGERATION SYSTEM DESIGN

A. System Description

The refrigeration system for the magnet will be similar to that developed at LBL for the TPC solenoid.[1] Such a system is also used on CELLO.[2] The system is shown in Figure V-1.

The magnet helium system consists of an aluminum cooling coil attached to either the aluminum bobbin or the banding. The tubing may be either spiral or longitudinal wound with a tube separation of 30 cm. The tubing is a 2cm x 2cm extrusion with attachment lugs and has adequate wall thickness (2mm) for the expected quench pressures. Approximately 160m of tubing are required.

The cooling coil leads to a control dewar with subcooler, the function of which is to provide cold gas for the current leads, allow single-phase heat exchange, monitor the refrigeration system, and serve as a liquid buffer volume.

Liquid nitrogen cooled shields are provided both inside and outside of coil.

Given this basic design and a 25K temperature differential on the shields, the steady state load on the refrigeration system is $\sim$ 8 watts. The charging load (for 5 min charge or discharge) is approximately 30 watts. The maximum ΔT and ΔP encountered in the cooling tube as a consequence of a 30W load are .1K and 2 psi respectively.

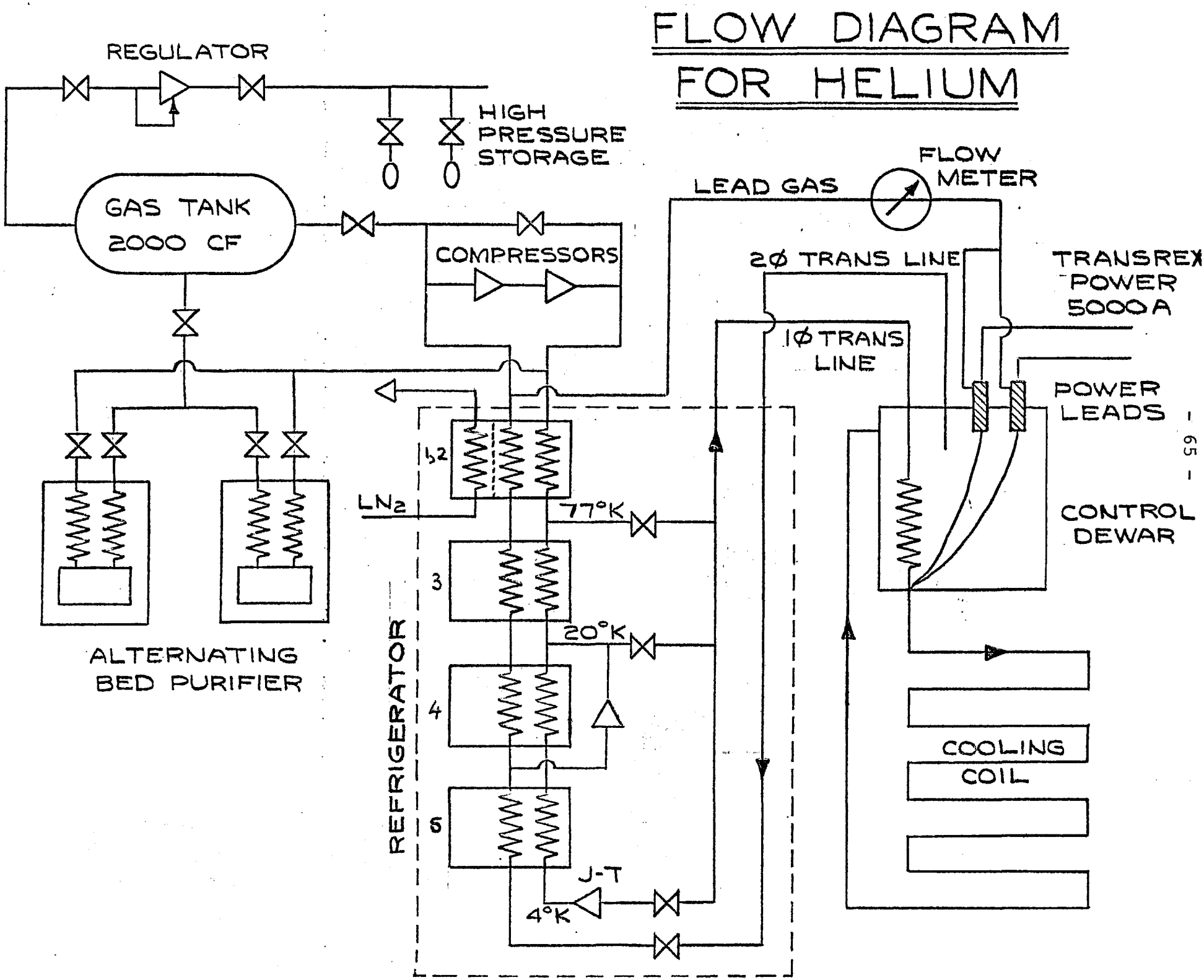

FIG. V-1 Refrigeration System Schematic

In this conceptual study an Energy Doubler satellite refrigerator was assumed as the source of refrigeration. Design parameters were determined from the 700W refrigerator capacity and a maximum coil temperature of 4.6K.

B. Magnet Cool Down

The cold mass of the solenoid is 3,500kG, which corresponds to a total enthalpy change from 4.2K to 300K of 7×10^8 J.

The magnet and refrigerator are cooled down together. This allows good Carnot efficiency and makes large cooling power available. With a satellite refrigerator, about 9kW from expansion engines and 6kW from liquid nitrogen are available. If we allow a 10 atm pressure drop across the cooling coil, 5kW of cooling power and a mass flow equal to 20% of the compressor capacity, we obtain an input to output cooling coil temperature difference of 50K. This differential is practically constant from 300K to 80K. The dissipative processes involved are: by the coil itself, about 1kW and by frictional power loss amounting to 1.2kW on the average.

With a system enthalpy of 7×10^8 J we obtain a cooldown to 80K of roughly 2 days. After the coil has reached 20K or so, liquid helium can be introduced into the system to speed the cooldown. A temperature

of 4.2K is reached in an additional 6 hours or less. Radial temperature gradients during cooldown of no more than 1K are maintained across the coil/structure.

C. Steady State Operation of the Magnet

As soon as sufficient liquid has accumulated in the control dewar, the magnet can be energized. In steady state operation, liquid is subcooled to 4.5K and delivered at quality X = 0 (100% liquid). With a mass flow of 10gm/sec and a quality of .2 at the outlet, one can extract 30W from the coil with a Δ T less than .1K and ΔP less than 2 psi. Frictional (convection) load is negligible in terms of refrigeration. The effect of thermal radiation and thermal conductivity of materials between the liquid and the coil have been included in the calculation.

D. Magnet Warm Up

The refrigerator is warmed up simultaneously with the magnet. The refrigerator compressors supply preheated gas to the refrigerator cold box and magnet cryostat. Since very large mass flows are available ($\sim$ 40 grams/sec) and since a 10 to 20kw heater could be used, the system could be warmed up in approximately 24 hours.

E. System Upset

Following a magnet quench, the liquid in the cooling tube (60ℓ) will vaporize and the pressure in the control dewar will rise. Depending on the size of the ullage and the pressure ratings of the vessels, some fraction of the 60ℓ may be vented.

F. 80K Refrigeration System

Liquid nitrogen cooled shields are used to reduce the thermal radiation heat load to the magnet. The shields are fabricated from sheets of aluminum alloy, slit axially to eliminate eddy currents during charging or quench. By cooling each end of the shields with a loop containing nitrogen, the temperature gradient to the centers will not exceed 25K with adequate super-insulation between the vacuum vessel and the shield. The liquid nitrogen manifold is gravity fed forced-flow and provides refrigeration to heat-intercept the coil supports. The total nitrogen consumption of the shield system is about 7 ℓ/hr.

REFERENCES

1. M.A. Green, "The Development of Large High Current Density Superconducting Solenoid Magnets for Use in High Energy Physics Experiments", Lawrence Berkeley Laboratory Report, LBL-5350, May 1977.

2. P. Komarek & H. DesPortes, "Magnetic Field System for PETRA Experiment", SACLAY Report, STIPE/76-52, July 1976.

VI. SYSTEM PARAMETERS

General

Cryostat inner diameter:	2.74 m (108")
Cryostat outer diameter:	3.0 m (118")
Cryostat length:	5.0 m (197")
Central field:	1.5T

Coil

Coil inner diameter:	2.84m (112")
Coil circumference:	8.92m (29.3')
Coil winding length:	4.90m (193")
Winding scheme:	Single layer helical level - wind
Stored Energy:	30×10^6 J @ 1.5T
Operating Current:	5,000A @ 1.5T
Inductance:	2.4H
Peak field at conductor:	1.73T
Dump resistor:	0.1 - 0.3Ω
Charge time:	5 min.
Required linear current density:	1200 A/mm @ 1.5T
Design linear current density:	1320 A/mm

Conductor

General:	Soldered Al/Cu/NbTi
Overall dimensions:	3.79m (0.149") x 10.56 (0.416")
Total insulation thickness (turn-to-turn):	0.2mm (0.008")
Bare dimensions:	3.59mm (0.141") x 10.36mm (0.408")
Number of turns:	1293
Al:Cu:Nb-Ti area ratios:	11.7:1.8:1.0

Bare conductor current density:	134 A/mm^2 = 1.34 x 10^8 A/m^2
Cu/NbTi Composite	
Alloy:	Nb 46.5 a/o Ti
Matrix:	Copper ASTM B170-1; CDA 101
Short Sample Current:	7,700 A @ 2T, 4.2K
NbTi Short Sample Current Density:	3,000 A/mm^2 (3 x 10^9 A/m^2) @ 2T, 4.2K
Bare Width:	3.59 mm (0.141")
Bare Thickness:	2.0 mm (0.078")
Cu:NbTi Area Ratio:	1.8
No. Filaments:	2,400
Filament Diameter:	$\sim$ 35 μm
Twist Pitch:	12.7 mm (1/2 inch)
Length Required:	$\sim$ 12km (39,000 ft.)
Weight:	$\sim$ 640kg (1,400 lb.)
Aluminum	
Alloy:	99.995 + %
Residual Resistivity Ratio:	> 1,000
Strip Width:	8.36mm (0.329")
Strip Thickness:	3.59mm (0.141")
Preparation:	copper and solder electroplated
Weight:	1,000kg (2,200 lb.)
Cryostat	
Inner vacuum vessel material/ thickness:	Al/6.35 mm (0.25")
Inner radiation shield material/ thickness:	Al/1.6 mm (0.0625")

Outer radiation shield material/thickness:		Al/1.6mm (0.0625")
Outer vacuum vessel material/ thickness:		Welded Al extrusions
Insulation:		High vacuum plus multilayer insulation

Cryogenics/Refrigeration

Cooling mode:		Single phase LHe in tubes
Cooling tube:	Orientation:	longitudinal or spiral
	Separation:	30 cm (1 foot)
	Inner dia.:	20 mm (3/4")
	Total Length:	160m (525 feet)
Cold mass:		Cu/NbTi, 640 kG, Al 3,000 kG
Cooldown Time:		300K → 80K ≤ 2 days 80K → 4.2K ≤ 12 hours
Steady-state heat load:		∿ 10W
Charging heat load:		∿ 30W
Single phase mass flow:		∿ 10 gm/sec
Maximum steady-state coil temperature:		∿ 4.6K

Forces

Total compressive axial force at mid-plane:	1.1×10^6 N (2.47×10^5 lb)
Axial decentering force:	240 N/cm (137 $\frac{lb}{in}$) at 1/2" displacement
Radial decentering force:	1.6×10^5 N/cm (9.1×10^4 $\frac{lb}{in}$) at 1/2" displacement

Iron Yoke

Total weight:	1,000 ton
Weight of end plugs:	200 ton

Radiation Thickness

Item	Prestressed Design		No Prestress - Integral Conductor/Banding		No Prestress - Sheet Banding	
Inner Vacuum Vessel	0.635cm	.071λ	.635cm	.071λ	.635cm	.071λ
Inner Shield	0.160cm	.018λ	.160cm	.018λ	.160cm	.018λ
Coil Bobbin	1.10 cm	.122λ	.300cm	.033λ	.318cm	.018λ
Cu/NbTi	0.20 cm	.125λ	.20 cm	.125λ	.20 cm	.125λ
Pure Aluminum	0.84 cm	.093λ	.84 cm	.093λ	.84 cm	.093λ
Banding	1.03 cm	.114λ	.923cm	.103λ	.923cm	.103λ
Outer Shield	0.160cm	.018λ	.160cm	.018λ	.160cm	.018λ
Outer Vacuum Vessel	---	.054λ	--	.054λ	--	.054λ
Superinsulation, Cooling, tubes, etc.	---	.045λ	--	.045λ	--	.045λ
Total:		0.660λ		0.560λ		0.545λ

Values of the thickness of material equivalent to one radiation length are found in LBL-535 (M.A. Green) Page 14.

VII. CONSTRUCTION SCHEDULE

It is estimated that the magnet could be designed, fabricated, and tested in approximately two years. A more exact time schedule can be determined after the decisions regarding design and fabrication responsibility and manpower committment have been made.

VIII. COST ESTIMATE

Materials

Item	Material	Amount	Unit Cost	Cost
Inner vacuum	Al	1700 lb (773 KG)	$2.00/lb	3,400
Inner shield	Al	220 lb (100 kg)	$2.00/lb	500
Coil bobbin	G-10	--	--	20,000
Superconductor	Al:Cu:NbTi	15km		100,000
Cooling tube	Al	160 m		2,000
Outer shield	Al	232 lb (105 kg)	$2.00/lb	500
Outer vacuum	Al	--	--	5,000
Lead box	--	--	--	3,600
Supports	G-10	--	--	5,000
			TOTAL MATERIALS	$140,000

Fabrication

Estimate fabrication cost at three times material cost.	$420,000

Electrical System

Power Supply (5000A, 50V)	20,000
Instrumentation, control	30,000
	$50,000

Fixturing

Coil Winding	50,000
Vessel Assembly	50,000
	$100,000

Cryogenic System

Transfer Lines & Control Dewar	15,000
Cryogenics Control	10,000
Nitrogen System	20,000
	$45,000

Summary

Materials	$140,000
Fabrication	$420,000
Electrical	$ 50,000
Cryogenics	$ 45,000
Fixturing	$100,000
TOTAL:	$755,000

IX. PROTOTYPE DEVELOPMENT

We have considered three types of prototype work:

1. Measurements of the properties of superconducting or pure Al wires under various conditions of cyclic strain at the University of Wisconsin Test Facility.
2. Construction of a small prototype magnet.
3. Early fabrication of the superconducting wire for the magnet and tests of this wire.

We now describe some of the details of these tests.

A. Wisconsin Strain Tests

There is a test setup at Wisconsin to measure thermal and electrical properties of materials that are strained in a magnetic field. Figures IX-1 and IX-2 shows some of the details of the test setup.

It is important to perform mechanical and electrical tests on high purity aluminum which are relevant to the design of the magnet. A verification of the strain-dependent resistivity of aluminum similar or identical to that used for the actual conductor is of primary importance. Tests of the plastic behavior of such aluminum, when stressed beyond yield, with actual $\vec{J} \times \vec{B}$ forces are also desirable. Since the presence of superconducting material only complicates the RRR measurements, it is initially proposed to use available aluminum of relevant purity in the tests. The prototype conductor will be tested when it becomes available. In detail the initial tests will consist of:

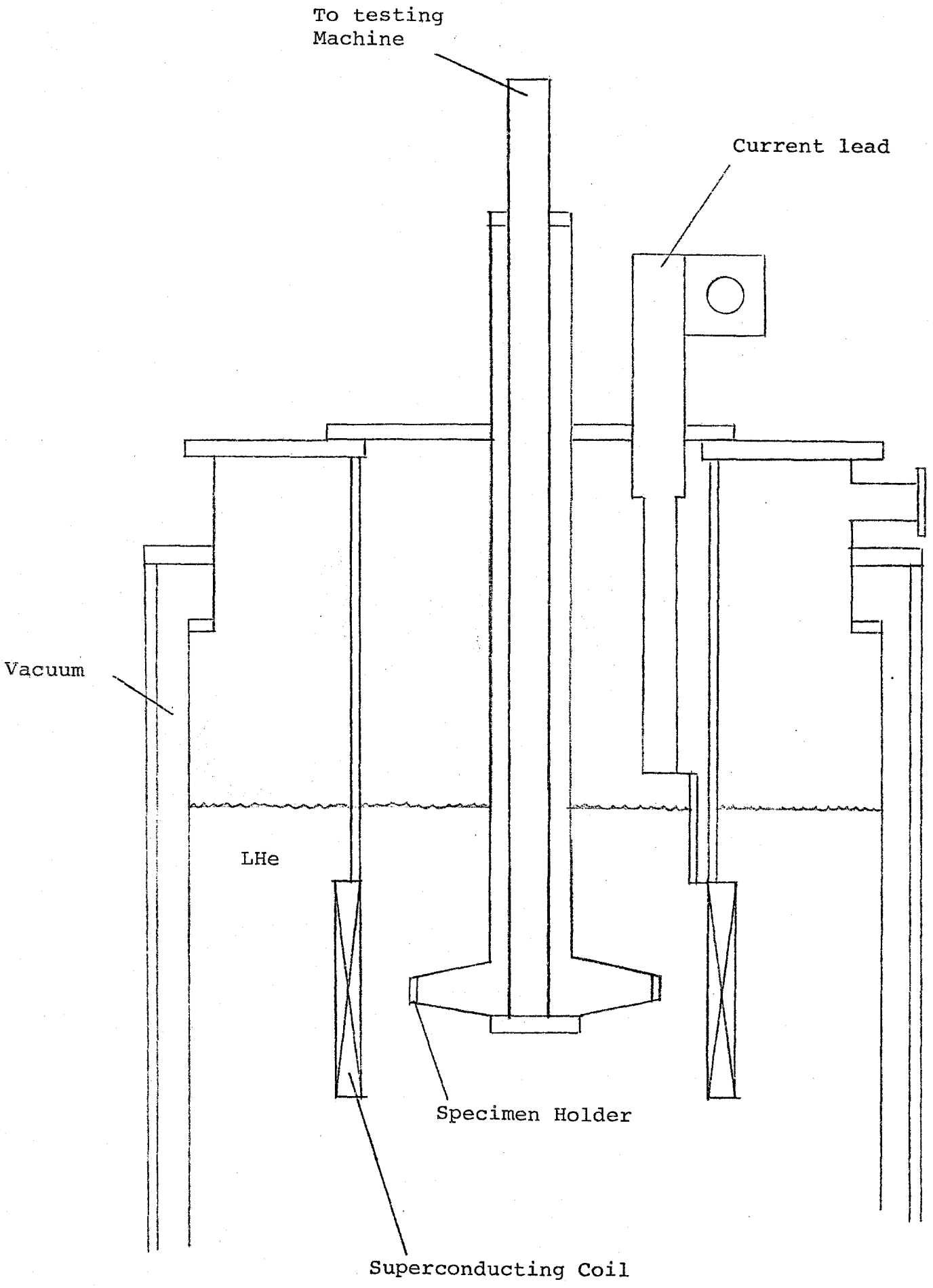

FIX IX-1 University of Wisconsin Test Apparatus

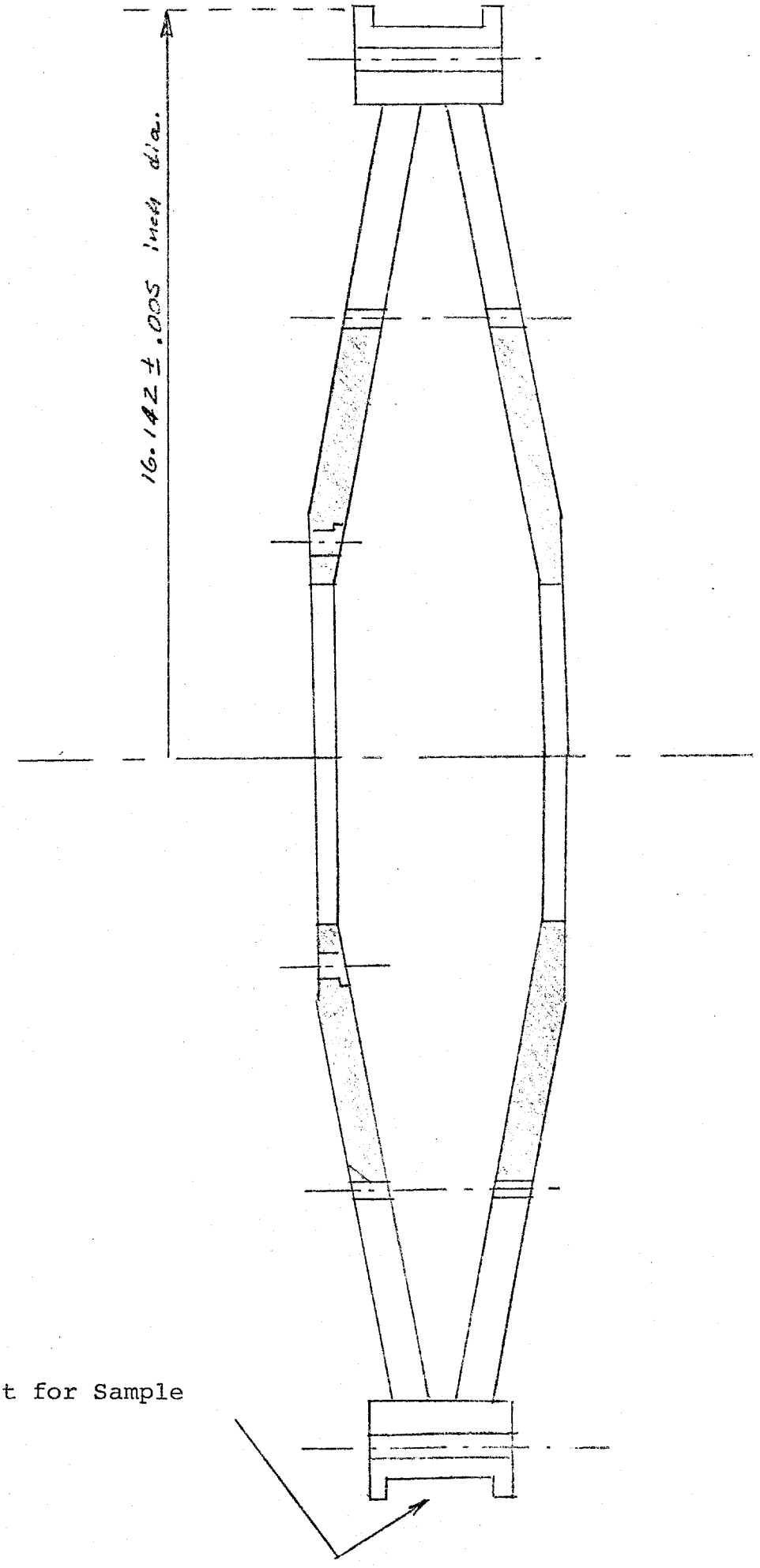

FIG. IX-2 University of Wisconsin Test Apparatus, Details

Test Specimen #1

1. Measure RRR of the as-received material.

2. Wind onto aluminum bobbin with interturn insulation of wet layup epoxy fiberglass.

3. Measure RRR as wound.

4. Anneal, measure RRR.

5. Apply cyclic strain at zero field.
Measure RRR at 1, 10, 100, 500, 1,000 cycles for $\varepsilon = 0.1\%$.
Repeat for $\varepsilon = 0.2\%$, 0.3%, and 0.4%.

6. Anneal, measure RRR. Inspect coil.

7. Operate with heavy current in conductor, in magnetic field. Measure RRR. Inspect coil.

Test Specimen #2

1. Repeat steps 2 - 6 for a coil wound with banding (no prestress). Use same wet-layup for winding procedure.

B. Prototype Coil Construction

We have considered the pros and cons of constructing a test coil to assist with the final design and reduce the risks involved in the extrapolation from the present generation of detector solenoids.

Pro

-- The model coil will incorporate the first conductor sample manufactured for the magnet and will serve as a useful test of that conductor.

-- The model coil will give vital information about the stability limits, particularly during charging, of the conductor design.

-- The model coil will test the winding design and insulation scheme chosen for the coil.

-- The model coil will give important information about the quench behavior of the winding design.

-- The model will assist in the cryogenic system design.

-- The model, if large enough, will provide valuable winding and construction experience relevant to the full-size magnet. This includes conductor joints and end terminations, cryogenic system details, current lead details, etc.

-- The model might be designed to operate at the hoop stress levels of the full-size magnet. This is not completely essential as this stress is perhaps easy to calculate and design for. The decision would depend on how much test conductor and time were available and if a test vacuum box could be located.

Con

-- The CELLO magnet should provide adequate information about magnets of this type, so that the extrapolation in size is essentially without risk.

-- The cost of a prototype and delay in schedule may be prohibitive.

-- A small model coil will not achieve hoop stresses as large as those in the full size magnet.

C. Prototype Conductor Development

It is proposed to purchase a length of prototype conductor prior to committing funds for the conductor for the solenoid. This conductor could be used for short sample, RRR and strain/resistivity tests, for a model coil if desired, and for practice winding. The proto-conductor would be identical to that proposed for the large solenoid. The procurement of the proto-conductor would also serve to qualify the vendor and to permit him to set up an assembly line.

The conductor would be fabricated using techniques developed at CEN-Saclay for the CELLO conductor. The successful vendor would pruchase the pure aluminum, copper and solder electroplate it, and bond it to the tinned CU/NbTi composite provided by Fermilab. Specifications have been written for the proto-conductor. It is the intention of Fermilab to solicit proposals for the proto-conductor as soon as possible.

A. Stress Analysis of Coil with Prestressed Banding

We outline a stress calculation as an example. We consider here in detail the "pre-loaded" design that is similar to the CELLO magnet and has an Al bore tube. Throughout this analysis we will ignore the high purity aluminum.

Dimensions and Loads

Radius at conductor = 1.5m = 60 inches.

Length = 5m $\sim$ 200 inches

Magnetic loading = 1.5 tesla $\sim$ 130 psi (0.9MPa) equivalent.

Definitions

t_B = banding thickness

t_b = bobbin (bore tube) thickness

t_c = thickness of Cu/NbTi composite

σ_{Bo} = initial banding stress

σ_{bo} = initial stress in bore tube

σ_{co} = initial stress in Cu/NbTi composite

$\sigma_{Bc} = \sigma_{bc}$ = cooldown stress in aluminum parts

σ_{cc} = cool down stress in composite

σ_{Bm} = electromagnetic stress in banding

σ_{bm} = electromagnetic stress in bore tube

σ_{cm} = electromagnetic stress in composite

σ_{Bf} = final stress in banding

σ_{bf} = final stress in bore tube

σ_{cf} = final stress in composite

Cu/NbTi Composite

Assumptions:

The composite is wound with zero winding tension.

Alloy Aluminum Banding

Assumptions:

A maximum strain of 0.004 or 0.4%, giving a nominal maximum stress of 40,000 psi.

The banding is wound under tension, which prestresses both conductor and bore tube into compression.

That under magnetic loading the bore tube is still under a nominal compression to maintain good thermal contact with the conductor.

Then: Minimum banding thickness, $t_B = \frac{130 \text{ psi} \times 61"}{40{,}000 \text{ psi}} = 0.198"$

$= 0.504$ cm.

Bore Tube or Bobbin

Assumptions:

The bore is reinforced or braced radially during the winding. The braces are removed after construction but bore tube remains in place.

An aluminum alloy bore tube is used with bolted on or welded end flanges to produce axial prestress in conductor layer and to carry any axial load from radial magnetic fields.

The design of the bore tube involves the consideration of several conditions or loadings. These are listed below with factors or formulas for each.

During winding, assembly, and shipping, the bore tube must not buckle radially due to the winding tension of the conductor and alloy banding. A formula given on page 535 of the 5th edition of "Formulas for Stress and Strain" by Roark and Young applies to this case.

$$\frac{P_o}{AE} = -2.67\ (\frac{k}{r})^{1.2} \qquad (1)$$

Here P_o is a conservative value of the buckling hoop compressive force with no friction between the inner buckling ring and the surrounding banding where A is the bore tube cross sectional area, E the modulus, k the radius of gyration of the cross section, and r the radius of the ring. The formula is conservative and little of the buckling stress comes from the winding of the conductor and the conductor is bonded to the bore tube. Therefore,we will use a factor of safety of 1.5 and add the superconducting portion of the "Cello" type conductor to the bore tube when calculating A and k. The bore tube must also carry axial tension to prestress the conductor layer in compression axially. It must be thick enough at the ends to allow bolting of the axial clamps.

The bore tube also enters into the axial stiffness of the entire assembly when considering the decentering magnetic forces.

Now carry out the calculations for the bore tube thickness based on the assumptions and factors listed above.

Let σ_{bo} be the initial bore tube stress due to winding the banding under pretension. Assume the conductor strains like the bore tube and forms a part of the cross section during winding.

$$\sigma_{bo} = P_o/A \qquad (2)$$

Cross section dimensions and properties:

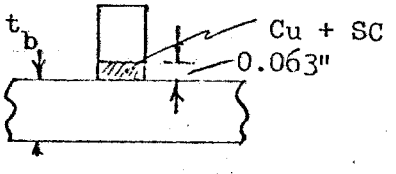

Take a 1" representative length and work out an equivalent section. Let E (Cu/NbTi) = 15 x 10^6 psi. Let E(aluminum) = 10 x 10^6 psi.

Equivalent section of aluminum material

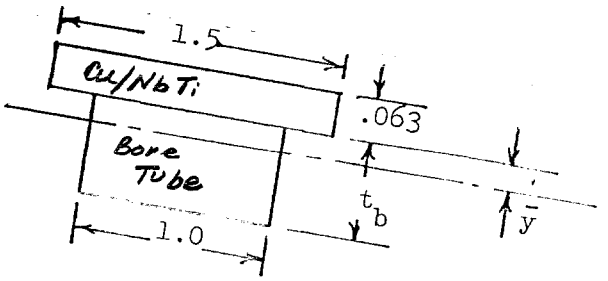

$$\bar{y} = \frac{\frac{tb^2}{2} - .0}{tL}$$

$$A = t_b + .0945$$

$$I_{NA} = 1/3t_b^3 + 1/3 \times 1.5 \times .063^3 + (t_b + .0945)\bar{y}^2$$

Table X-1

t_b	$\bar{y}$	I_{NA}	A	k	σ_{bo}	P_o
.2	.0578	.003775	.2945	.1132	-10,747	-3165
.25	.08206	.007653	.3445	.149	-14,947	-5149
.30	.1065	.0135	.3945	.186	-19,504	-7694
.35	.1311	.0220	.4445	.223	-24,248	-10,778
.40	.1558	.0335	.4945	.260	-29,153	-14,415
.45	.1805	.0482	.5445	.298	-34,337	-18,697
.50	.2052	.0668	.5945	.335	-39,516	-23,492

$$\sigma_{bo} = \frac{-E}{1.5} \times 2.67 \left(\frac{k}{r}\right)^{1.2} = \frac{-10 \times 10^6}{(1-.33^2)} \frac{2.67}{1.5} \frac{k^{1.2}}{60^{1.2}}$$

$$= -1.458 \times 10^5 k^{1.2}$$

If the bore tube (equivalent) is in equilibrium with the banding, then the banding initial

stress, σ_{Bo}, is given by:

$$\sigma_{Bo} \times 0.198 + P_o = 0 \qquad (3)$$

Cool Down Stresses

During cool down let the change in stress in the aluminum structural parts be given by σ_{Bc} and σ_{bc} and in the Cu/NbTi Composite by σ_{cc}.

The unit length change in the banding and bore tube is then:

$$-4.2 \times 10^{-3} + \frac{\sigma Bc}{10 \times 10^6} = \Delta\varepsilon_{Bc} \qquad (4)$$

$$-4.2 \times 10^{3} + \frac{\sigma\, bc}{10 \times 10^6} = \Delta\varepsilon_{bc} \qquad (4')$$

For the composite:

$$-2.9 \times 10^{-3} + \frac{\sigma\, cc}{15 \times 10^6} = \Delta\varepsilon_{cc} \qquad (5)$$

For equilibrium:

$$\sigma_{Bc}(t_b + t_B) + \sigma_{cc} \times .063 = 0 \qquad (6)$$

And since:

$$\varepsilon_{Bc} = \Delta\varepsilon_{bc} = \Delta\varepsilon_{cc}$$

$$\sigma_{bc} = \sigma_{Bc}$$

$$\sigma_{cc} = 1.5\, \sigma_{Bc} - 19{,}500 \qquad (7)$$

Solving (6) and (7):

$$\sigma_{Bc} = (t_b + t_B) + .063\,(1.5\, \sigma_{Bc} - 19{,}500) = 0$$

or, $$\sigma_{Bc}\,(t_b + t_B + .0945) = 1{,}229 \qquad (8)$$

and, $$\sigma_{Bc} = 1{,}220/(t_b + t_B + .0945)$$

also, $$\sigma_{cc} = 1.5\sigma_{Bc} - 19{,}500 \qquad (9)$$

Electromagnetic Stresses

During the magnetic loading, the effective area carrying the load assuming the bore tube does not go into tension is given by:

$$A_{eff} = t_b + t_B \frac{15x10^6}{10x10^6} \times .063 = t_b + t_B + .0945$$

$$\sigma_{bm} = \sigma_{Bm} = \frac{130 \text{ psi} \times 61"}{t_b + t_B + .0945} = \frac{7930}{t_b + t_b + .0945} \quad (10)$$

and, $$\sigma_{cm} = 1.5\sigma_{bm} \quad (11)$$

Calculations

We can now set up a table to solve these equations by trial and error. We will first assume a value for σ_{Bo}, the winding tensile stress in the banding remembering that $t_B = 0.198"$. The results are given in Table X-2. The cases with σ_{Bo} equal to 20,000 and 25,000 are not valid solutions since $\sigma_{bf} > 0$. The case of 30,000 psi pretension appears to be a marginal solution and we can start from here to determine a more exact solution including the insulation, etc. Winding the conductor with a slight pretension would reduce the rather large compressive stresses in the Cu/NbTi. A winding tension of 150 lbs. would result in a final stress of essentially zero. The strain in the pure aluminum is estimated to go from -0.0015 (compression) to approximately zero when the field is energized.

TABLE X-2

ANALYSIS OF PRESTRESSED COIL

Initial Stresses						Cooldown Stresses		Magnetic Stresses		Final Stresses		
σ_{Bb} (psi)	P_o (Eq. 3)	t_b (Table X-1)	σ_{bo} (Eq. 2)	t_B	σ_{co}	$\sigma_{Bc} = \sigma_{bc}$ (Eq. 8)	σ_{cc} (Eq. 9)	$\sigma_{Bm} = \sigma_{bm}$ (Eq. 10)	σ_{cm} (Eq. 11)	$\sigma_{Bf} = \sigma_{Bo} + \sigma_{Bc} + \sigma_{Bm}$	$\sigma_{bf} = \sigma_{bo} + \sigma_{bc} + \sigma_{bm}$	$\sigma_{cf} = \sigma_{co} + \sigma_{cc} + \sigma_{cm}$
20,000	-3,960	0.22"	-12,591	0.198"	-18,885	2,398	-15,900	15,473	23,210	37,871	5,280	-11,576
25,000	-4,950	0.245"	-14,580	0.198"	-21,870	2,287	-16,070	14,753	22,130	42,040	2,460	-15,810
30,000	-5,940	0.266"	-16,477	0.198"	-24,716	2,200	-16,199	14,199	21,299	46,399	- 78	-19,200

Summary of Thicknesses and Radiation Lengths

Band t_B = .198" Bore Tube t_b = .255"	.453"	l_r = .056
Conductor/Aluminum = .354"		l_r = .100
Cu/NbTi = .063"		l_r = .100
Total:		.331

B. Stress Analysis of Coil with Non-Prestressed Banding

Dimensions and Loads

R = Coil radius at conductor = 56"

p = Magnetic Loading at 1.5 T = 130 psi

E(aluminum) = 11×10^6 psi

E(Cu/NbTi) = 15×10^6 psi

E(epoxy-fiberglass) = 3×10^6 psi

Definitions and Assumptions

σ_{Bo} = initial stress in banding = 0

σ_{bo} = initial stress in bobbin = 0

σ_{co} = initial stress in composite = 0

ε_B = final strain in banding

= final strain in pure aluminum = 0.002

σ_{Bf} = final stress in banding

w = axial length of unit cell

A_{eq} = equivalent area of unit cell

Coil Cross Section

Consider the unit cell:

Not to scale.
All dimensions in inches.

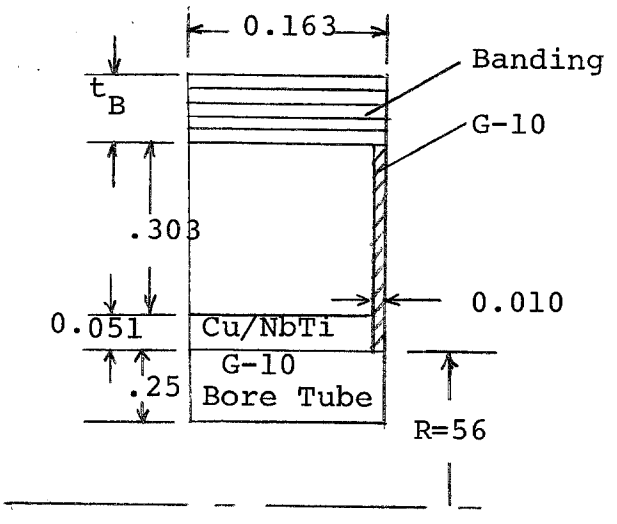

Conductor Bonded to Bore Tube

$$\sigma_{Bf} = \varepsilon_B E(\text{aluminum}) = (0.002)(11 \times 10^6) = 22{,}000 \text{ psi} \quad (1)$$

but

$$\sigma_{Bf} = \frac{pwR}{A_{eq}} = \frac{(130 \text{ psi})(0.163")(56")}{A_{eq}} = \frac{1187}{A_{eq}} \quad (2)$$

so

$$A_{eq} = \frac{1187}{22{,}000} = 0.054 \quad . \quad (3)$$

From geometry

A_{eq} = equivalent area of banding + bore tube +

+ Cu/NbTi composite + insulation

$$= 0.163\ t_B + (0.25)(0.163)(3/11)$$

$$+ (0.153)(0.051)(15/11) + (0.354)(0.01)(3/11)$$

$$= 0.163\ t_B + 0.023 \text{ in}^2 \quad (4)$$

Substituting (3) into (4)

$$t_B = 0.190" = 0.482 \text{ cm.}$$

Conductor Not Bonded to Bore Tube

$$A_{eq} = .163_{tB} + .153 \times .051 \times \frac{15}{11} + .354 \times .01 \times \frac{3}{11}$$
$$= .163_{tB} + .012$$

and $t_B = .257$ in = 6.5mm

Ignore Conductor and Insulation

$A_{eq} = .163\ t_B$ and $t_B = .331$ in = 8.41mm

Allowing for a 10% higher magnetic field $t_B = 9.25$mm.

C. Stability of Outer Vacuum Can Using Welded Aluminum Extrusions

Construction

The vessel is constructed of 46 extrusions having the cross section shown in Fig. X-1 which are edge welded to form a 46 sided polygon. We will treat it as a cylinder.

Summary

Circumferential moment of inertia = 0.00995 in^4/inch

Longitudinal moment of inertia = 0.0108 in^4/inch

For an infinitely long shell q' = buckling pressure = 1.74 psi with a half wave length of 92".

For a finite shell held round at midlength and at the ends q' = 36.2 psi with a half wave length of 20".

For a 20" half wave length lateral shear is important.

Corrected for lateral shear q' = 28 psi.

Detailed Calculations

For shell buckling in a circumferential direction, the effective moment of inertia is given by

$$I = \frac{1}{12}(0.617^3 - 0.487^3) = 0.00995 \text{ in}^4\text{/inch of length.}$$

For an outer radius, R = 57", the mean radius, r = 59-0.617/2 = 58.692.

If this were an infinite cylinder or a very long cylinder, the theoretical critical external pressure q' would be given by,

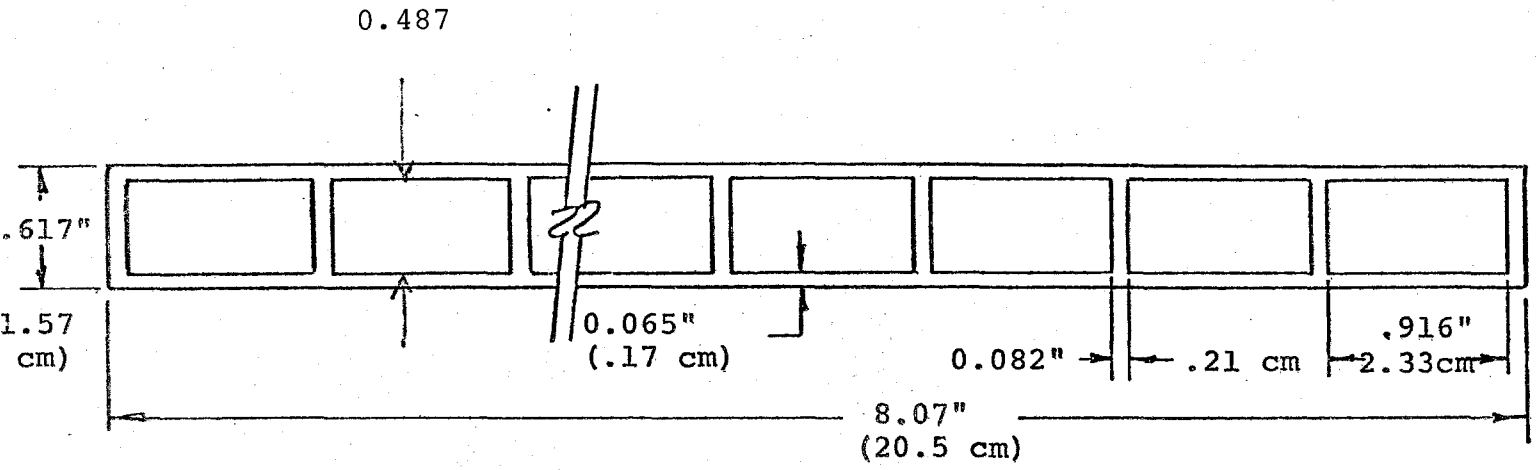

Fig. X-1

ALUMINUM EXTRUSION USED FOR OUTER VACUUM VESSEL.

$$q' = \frac{3EI}{(1-\nu^2)r^3} = \frac{3 \times 10.5 \times 10^6 \times 0.00995}{(1-0.33^2) \times 58.692^3} = 1.74 \text{ psi} \quad (1)$$

with a half wave length equal to one quarter the circumference or 92.19".

Since we will try to brace the outer vacuum can to maintain a circular shape at midlength as well as at the ends the critical buckling pressure can be found by case 19b on page 556 of "Formulas for Stress and Strain", 5th Edition by Roark and Young,

$$q' = 0.807 \frac{Et^2}{\ell r} \sqrt[4]{\left(\frac{1}{1-\nu^2}\right)^3 \frac{t^2}{r^2}} \quad . \quad (2)$$

Since Eq. (2) is for a solid plate and buckling is accomplished by bending in both circumferential and axial directions, we will evaluate the moment of inertia for bending the wall in the axial direction.

For an 8.07 inch width

$$I = \frac{1}{12} \times 8.07 \times 0.617^3 - \frac{1}{12} \times 0.9165 \times 0.487^3 \times 8 = 0.0874 \text{ in}^4/\text{inch}$$

for an 1-inch width,

$$I = \frac{0.0874}{8.07} = 0.0108 \text{ in}^4/\text{inch}.$$

If we assume that the buckling wave lengths are approximately equal in the circumferential and axial directions, the energy absorbed will be proportional to the moment of inertia I. We will use an average value of I ,

$$I_{ave} = (0.00995 + 0.0108)/2 = 0.0104 \text{ in}^4/\text{inch}.$$

To apply Eq. (2) we can use an equivalent thickness given by $I = \frac{t^3}{12}$ or $t = \sqrt[3]{12I}$, so

$$t_{eq} = \sqrt[3]{12 \times 0.0104} = 0.4993$$

also let

ℓ = 100 inches.

Then q' = 36.2 psi.

Since q' will vary approximately as the square of the wave length, the new wave length = $92 \times \sqrt{\frac{1.74}{36.2}} = 20.2"$.

This is about 2-1/2 panel widths. For this short a wave length, the effect of transverse shear will possibly become important. This can be treated as a sandwich cylinder but not easily. Another approach is to see how much reduction in critical load is caused by shear if this panel is used as a pinned load column with a length of 20.2". For this, see Eq. (2-65) on page 140 of "Theory of Elastic Stability" by Timoshenko and Gore, second edition.

Without the effect of lateral shear, the value of P_{cr} is given by

$$P_{cr} = \frac{\pi^2 EI}{\ell^2} \quad . \tag{3}$$

When shear is included, the expression becomes

$$P_{cr} = \frac{\pi^2 EI}{\ell^2} \left\{ \frac{1}{1 + \frac{\pi^2 EI}{\ell^2} \left[\frac{ab}{12EI_b} + \frac{a^2}{24EI_c} \left(\frac{1}{1-\alpha}\right) + \frac{na}{GA_b G} \right]} \right\} \tag{4}$$

where

$$G = \frac{10.5 \times 10^6}{2(1.33)} = 3.95 \times 10^6$$

$$a = 0.9165 + 0.082 = 0.9985",$$

$$b = 0.617 - 0.065 = 0.552, \qquad A_b = 0.082$$

$$I_b = \frac{1}{12} \times 0.082^3 = 45.95 \times 10^{-6}$$

$$I_c = \frac{1}{12} \times 0.065^3 = 22.89 \times 10^{-6}$$

$$\alpha = \frac{P_{cr}}{2\pi^2 E I_c / a^2} \qquad n = 1.2$$

Since α contains P_{cr}, Eq. (4) is solved by trial and error. The solution $\alpha = 0.30$ and $P_{cr} = 2527(0.5326) = 1346$ psi is satisfactory.

It would seem reasonable but probably conservative to apply this same factor from Eq. (4), i.e., 0.5326, to the circumferential moment of inertia for the shell.

The new average moment of inertia is thus

$$I_{ave} = (0.00995 \times 0.5326 + 0.0108)/2 = 0.00805 \text{ in}^4/\text{inch}.$$

The new equivalent thickness is

$$t = \sqrt[3]{12 \times 0.00805} = 0.459 ,$$

and

$$q' = 27.7 \text{ psi} .$$

Any further iteration will raise the wavelength and reduce the effect of lateral shear so we will not recalculate at this time.

$$\text{Half wave length} = 92\sqrt{\frac{1.74}{27.7}} = 23.1 \text{ inches}.$$

A brace to the iron at the edge of every 8" piece of the extruded aluminum would give 3 supports per half wave and this

is adequate. The supports require a minimum stiffness (not strength),but we will not evaluate this minimum here.

D. Possible Assembly Procedure for Coil with Non-Prestressed Sheet Banding

1. Conductor Preparation: The large diameter storage spools are arranged according to length of conductor in spool, refrigerated if B-stage epoxy tape is used.

2. Tension Device for Winding: Duplicate CELLO and learn what can be improved. Winding tension to be nominal but not loose. Tensioning table also contains last cleanup of conductor to eliminate chips.

3. Insulation Scheme: With epoxy fiberglass bobbin only turn-to-turn is necessary. Insulate with .010" x .500" G-10 strip with care exercised so strip does not extend above conductor. Turn-to-banding insulation could be sheets of G-10 or Scotch-Ply epoxy tape.

4. The Winding Fixture: The fixture is like a lathe. A wooden mandrel supports the inside of the bobbin during winding. A box/beam frame will carry rotary tools along axis on a carriage for lathe type machining and later serve as conductor guide when winding coil. The bearing stands are convertible so that the winding fixture can be used as the assembly fixture to enable completion of the coil and cryostat in the same location and position. The winding space needed is 2-1/2 times the length of the coil ($\sim$ 40') with a crane not an absolute necessesity.

5. The Axial Preload of the Conductor: Should be adequate to "seat" insulation and squeeze out excess epoxy if coil is wound wet. Hydraulic clamps around the circumference could be used.

6. Coil End: Extra conductor is stored at each end for leads, temporarily secured to drum.

7. Splices in Conductor: Use lapped solder joint if possible, or butt weld on Cu/NbTi and aluminum separately. Can not have circumferential bumps or axial softness from splices.

8. Instrumentation: The fiberglass bobbin allows instrumentation wires to be put into the mold, ending at preselected points for voltage taps, thermocouples, or strain gauges. If bobbin is aluminum, care must be used so instrumentation leads do not short coil to ground.

9. Strain in Soft Aluminum: Care must be taken during winding to avoid unnecessary strain.

10. Winding Program and Winding Test Run: Coil bobbin cleaned thoroughly to eliminate chips and glass dust. Practice wind some number of turns to debug fixturing and procedures. Wind final coil on bobbin with tension and axial compression determined with practice winding. Heat to 100 - 120°C ($\sim$ 250°F) to cure any epoxy and to anneal winding strain in pure aluminum.

11. Check Finished Coil: Measure diameter of finished coil to see if outer surface is a circular cylinder.

12. Coil-Banding Insulation: Carefully measure circumference of "as built" coil. Cut ground insulation sheet (.020" G-10) to fit with minimal gap around circumference. One could also use Scotch-Ply or B-stage glass tape, spiral wound in sufficient number of layers to desired thickness.

13. Banding: Use carefully sheared strips of 48" wide aluminum 5053-T6 .050" thick with a radius on all edges. Sandblast both surfaces. Length of sheet determined from measured circumference less 1/4" to 1/2" gap. Apply epoxy to sheets and lay sheets around coil C-fashion down the length of coil. Use special hose clamps made from standard package steel banding strip, with riveted hose clamp ends, to hold sheets in place. Cure epoxy by heating with heat lamps or heating blankets. Rotate coil if necessary to avoid epoxy dripping out. Tighten hose clamps during curing to squeeze out excess epoxy. Additional sheets added one layer at a time using wet epoxy or B-staged epoxy sheet to obtain epoxy thickness 0.002" - 0.006". Stagger axial and circumferential gaps. Build up required banding thickness. Last banding layer is secured mechanically against glue failure by drilling holes in banding and using sheet metal screws.

14. End Rings and Axial Clamps: The banding at each coil end will be reinforced by an aluminum ring which is pinned and screwed into the banding. At this time the axial face of the banding is machined flush and coil ends prepared for axial clamp ring installation. Holes are drilled and taped in bore tube and ring using axial clamp ring as templete. Clamp rings installed to provide desired axial prestress on coil and banding.

15. Cooling Loop: The extruded cooling tube is routed on banding and secured to banding with epoxy and sheet metal screws. The "far end" coil lead is insulated and attached to cooling tube to reach the "near end" of coil. Leads and cooling tube ends should be long enough to reach control dewar about 6' above.

16. Stationary Leg Support: The rotating axle is removed and legs are fastened to axial clamp ring as temporary support.

17. Removal of Mandrel: The wooden mandrel is removed in segments and the inner surface of bore tube exposed.

18. Final Machining on Coil: Milling, machining of slots, drilling of holes for anchors, etc., done with inside and outside of coil accessible.

19. Instrumentation Wire: Installed through holes in bobbin.

20. Multilayer Insulation: A few layers of aluminized mylar applied to coil.

21. Installation of Radiation Shields: The thin aluminum shields with LIN tubes attached at the ends are installed at this time if they are supported to or through the coil. Care is taken since the shields are quite fragile.

22. Preparation of Vacuum Vessel: The vessel has been previously evacuated and strain gauge and deflection measurements made to check collapse stability. Multi layer insulation is applied.

23. Installation of Inner Vacuum Shell: Shell is slipped into coil as coil is supported from the outer

diameter. The radial support spokes are installed and adjusted. The axial midplane anchor is installed.

24. Installation of Outer Vacuum Shell and Control Dewar: The outer vacuum shell is slipped over the coil and inner vessel and temporary supports installed. The helium plumbing and electrical connections are made and routed through the transfer line to the control dewar. The vacuum vessel end caps are installed and welded in place.

25. Testing: Pressure, vacuum and electrical tests are completed prior to the first cool down.

XI. REPORT OF THE DESIGN REVIEW COMMITTEE

[A review of the above design was held at Fermilab on Sept. 11 - 12, 1978. The review committee consisted of P.H. Eberhard (LBL), Chairman; J.R. Purcell (General Atomic), R.L. Kustom (ANL), and D.E. Andrews (Cornell). The following is the report of this committee - Editor].

The attention of this committee has been focussed on the likelihood of success for the proposed design. We do not try to assess the pros and cons of all possible alternatives that might be considered for this project. We conclude that the proposed design approach could be made to work. More investigation of some parameters should be made and may require the design to be adjusted accordingly. The time to build such magnets is two years in general and a cost estimate around $ 1M is reasonable.

A. QUENCH PROTECTION

We noticed that the quench protection that is described in the report relies essentially on the value of the turn to turn quench propagation velocity. However, in the QUENCH program that value was arbitrarily assumed to be 22 cm/sec. We would like to recommend the following steps.

1. Design a turn to turn insulation that optimizes that value of transverse quench velocity. It would be advantageous if quench protection could be insured without an active external circuit.
2. Compute the value of that velocity using the physical constants of the material.
3. Check the theory of quench velocities using data provided by the CELLO magnet.
4. Design the coil to ground insulation such that the magnet

would withstand the voltages required to protect the magnet with an external circuit even if the transverse velocity were zero.

5. Test the final magnet inducing quenches at small current before energizing the magnet at full power.

Furthermore, we would like to encourage the designers to resolve the differences existing between different versions of the QUENCH program. Finally, a more realistic description of the quench should be used in their programs, not allowing current transfer to aluminum for 1 second or so in the beginning of the quench.

B. STABILITY

While we cannot be certain of an intrinsically stable magnet's ability to achieve the design field, we can make the following recommendations:

(1) Epoxy joints should be kept in compression, and the amount of epoxy used should be minimized.

(2) Limiting the strain in the high purity aluminum to 0.2% assures that its beneficial effects in transporting heat from a local disturbance are not lost.

(3) Care should be exercized in all stages of fabrication.

The proposal shows that these points are recognized by the magnet designers.

C. STRAY FIELD

We do not believe that the stray fields produced by this coil represent an essential problem. We do recommend that differences in the calculations of the stray field by different

programs be resolved, but in general expect that calculation of fields in highly saturated iron and with meshes of limited resolution are unreliable. Some estimate of the reliability may be obtained by trying different assumptions about the B vs. H curve of the iron. If possible, the design should be made flexible enough to allow additional magnetic shimming after the magnet has been constructed and field measurements made.

D. CHARGING TIME

We understand that a five minute charging time is a desirable requirement for the magnet, but it is not inflexible. The effects of eddy currents in the iron of large magnets are poorly understood at this time, but could be studied in either the existing Mark II coil at Stanford, or the CLEO magnet at Cornell (after about November of this year). Possibly the fields on the conductor will be different during charging than in a steady stable condition.

E. STRESS CONDITIONS

1. Stresses during cool down require further design analysis. Calculations which were presented were not checked by the committee. The committee recommends that an independent confirmation be made.
2. The effect of forces due to eddy currents during charging and discharging were tersely mentioned during the review. The complete study, if already undertaken, should be documented; if not, the study should be completed to be sure that the thin solenoid structure or nearby apparatus is not damaged by eddy current forces.

F. COOLING SYSTEM

The large refrigerator as proposed seems wasteful if it is dedicated only to the thin solenoid. Consideration should be given to use of a smaller dedicated refrigerator that more nearly matches the magnet load or sharing the large refrigerator with other devices.

A cooldown time of less than 2 days should not be the initial criteria. Instead let the thermal analysis of the coil system determine the cooldown time and if this is longer than desired consideration can be given to installing the coil while at $80^{o}K$.

G. SUPPORT STRUCTURE AND ASSEMBLY

1. The committee prefers prestressed narrow, spiral banding rather than large area "C type" shell bands; primarily because of the uncertainties associated with mechanical properties and effect on magnet stability.
2. The committee recommends against placing any ribs in the winding side of the bore tube which would interrupt the quench propagation.
3. The fiberglass bore tube has the advantage of eliminating any ground shorts through the bore tube. These advantages should be considered relative to the merits and weaknesses of other bore tube designs.

H. COSTS AND SCHEDULE

The costs as presented seem about right. The magnet without the refrigerator, iron and engineering will probably cost $1,000K. At this stage of the conceptual design it is not possible to obtain an accurate cost estimate.

The schedule as presented seems somewhat optimistic. It is clear that the finished conductor delivery is a critical path item and this procurement should be started as early as possible. The committee feels that it will take about 2 years to complete the magnet system.

I. WIRE FABRICATION

1. The committee agrees with the choice of conductor design and has no recommendations related to the fabrication.

J. GENERAL RECOMMENDATIONS

1. The design team should remain fully cognizant of CELLO progress.

2. Various splice techniques should be considered and fully tested.

3. Integrity and safety of the design of the magnet should be the main consideration of the construction rather than overly minimizing the radiation length.